

SUPERNOVA EXPLOSIONS IN ACCRETION DISKS IN ACTIVE GALACTIC NUCLEI:  
THREE-DIMENSIONAL MODELSA. MORANCHEL-BASURTO<sup>1</sup>, F. J. SÁNCHEZ-SALCEDO<sup>2</sup>, RAÚL O. CHAMETLA<sup>3</sup>, AND P. F. VELÁZQUEZ<sup>1</sup>*Draft version January 17, 2022*

## ABSTRACT

Supernova (SN) explosions can potentially affect the structure and evolution of circumnuclear disks in active galactic nuclei (AGN). Some previous studies have suggested that a relatively low rate of SN explosions can provide an effective value of alpha viscosity between 0.1 and 1 in AGN accretion disks within 1 pc scale. In order to test this possibility, we provide some analytic scalings of the evolution of a SN remnant embedded in a differentially rotating smooth disk. We calibrate our estimates using three-dimensional hydrodynamical simulations where the gas is modeled as adiabatic with index  $\gamma$ . Our simulations are suited to include the fact that a fraction of the momentum injected by the SN escapes from the disk into the corona. Based on these results, we calculate the contribution of SN explosions to the effective alpha viscosity, denoted by  $\alpha_{\text{SNe}}$ , in a model AGN accretion disk, where accretion is driven by the local viscosity  $\alpha$ . We find that for AGN galaxies with a central black hole of  $\sim 10^8 M_\odot$  and a disk with viscosity  $\alpha = 0.1$ , the contribution of SN explosions may be as large as  $\alpha_{\text{SNe}} \simeq 0.02$ , provided that  $\gamma \gtrsim 1.1$ . On the other hand, in the momentum conservation limit, which is valid when the push by the internal pressure of the SN remnant is negligible, we find  $\alpha_{\text{SNe}} \lesssim 6 \times 10^{-4}$ .

*Subject headings:* accretion, accretion disks – black hole physics – hydrodynamics – galaxies: active – quasars: general

## 1. INTRODUCTION

It is well established that the luminosity of the active galactic nuclei (AGN) is the result of gas being accreted by the central supermassive black hole (SMBH). In order to reach the central SMBH, the ISM gas must be transported from galactic scales down to the last stable orbit. At galactic scales, gravitational torques produced by bars and arms can bring the gas into the central sub-kpc region (e.g., Shlosman, Frank & Begelman 1989; Shlosman, Begelman & Frank 1990; Hopkins & Quataert 2011). At intermediate radii (scales 1-100 pc), the circumnuclear disk or torus, is gravitationally unstable. As a result, part of the gas turns into stars. It has been suggested that energy feedback from supernovae (SN) inside the circumnuclear disks may support a geometrically thick, turbulent circumnuclear disk (e.g., Wada & Norman 2002; Kawakatu & Wada 2008). Hobbs et al. (2011) suggest that feedback from stellar winds and SN within a kpc-scale disk can make the gas highly turbulent at “intermediate scales” and this turbulence can promote accretion (see also Hopkins et al. 2012).

At the pc and sub-pc scales from the nucleus, models predict the formation of a thin accretion disk surrounding the SMBH. Interestingly, reverberation mapping indicates that broad line regions (BLRs) in AGNs have a characteristic radial distance from 0.01 to 1 pc (e.g., Kaspi et al. 2007; Bentz et al. 2009; Du & Wang 2019), implying that BLRs overlap with the outer parts of the accretion disks. Understanding the interplay between the

underlying accretion disk, the BLR and the inner parts of the dusty torus is crucial in order to have a complete picture of the physical processes.

Models suggest that the accretion disk is gravitationally unstable between  $\sim 0.01$  pc and a few pc from the SMBH, and thus it is likely to fragment into clouds leading to a star-forming disk (e.g., Paczynski 1978; Shlosman & Begelman 1987; Collin & Zahn 1999; Collin & Huré 2001; Goodman 2003). Vigorous star formation could raise material from the surface of the underlying disk, feeding the BLR with metal-rich gas (Wang et al. 2012; Czerny et al. 2016). If so, the BLR can trace the metallicity of the accretion disk (Wang et al. 2011).

Emission-line flux ratios have been used to estimate the BLR metallicity. It has been found that, in many quasars, the BLR metallicity is very high, with typical values of 4–5 times solar (e.g., Hamann & Ferland 1993; Baldwin et al. 2003; Dietrich et al. 2003; Warner et al. 2003; Nagao et al. 2006; Kurk et al. 2007; Jiang et al. 2007; Juarez et al. 2009). The almost constant BLR line ratios over the redshift range suggests that such high metallicities were reached by a rapid and intense chemical enrichment at the cores of the host galaxies. However, the fact that the metallicity of host galaxies is generally lower than it is in BLRs, indicates that the BLRs have been enriched locally within the star-forming disk, rather than by the stellar population of the host galaxy (Wang et al. 2011).

A major long-standing puzzle is to explain how gas can power the central SMBH if a significant fraction of the gas in the radial inflow is consumed in forming stars. The problem of the consumption of gas can be alleviated if the angular momentum transport in the disk is efficient, i.e. if the effective  $\alpha$  viscosity is  $\gtrsim 0.1$  (Shlosman, Frank & Begelman 1989; Goodman 2003; Chen et al. 2009; Wang et al. 2010, 2011). Some authors have sug-

<sup>1</sup> Instituto de Ciencias Nucleares, Universidad Nacional Autónoma de México, CP 04510. Mexico City, Mexico

<sup>2</sup> Instituto de Astronomía, Universidad Nacional Autónoma de México, Ciudad Universitaria, Apt. Postal 70 264, C.P. 04510, Mexico City, Mexico

<sup>3</sup> Instituto de Ciencias Físicas, Universidad Nacional Autónoma de México, Av. Universidad s/n, 62210 Cuernavaca, Mor., Mexico

gested that repeated SN explosions in the star-forming disk, produce an effective viscosity  $\alpha \sim 0.1$  (Różyczka et al. 1995; Collin & Zahn 1999, 2008; Chen et al. 2009; Wang et al. 2010, 2011). However, there is still no consensus on the rate of SN explosions in the accretion disk required to provide  $\alpha \sim 0.1$ . The most detailed study on the amount of angular momentum redistributed by a single SN explosion in the accretion disk is given in Różyczka et al. (1995). Based on two-dimensional (2D) simulations, Różyczka et al. (1995) showed that the blast wave driven by a SN explosion deflects the trajectory of disk gas elements, resulting in an outward angular momentum flux, because the mixing between elements that have acquire angular momentum with those that have lost angular momentum is small. They argued that a SN rate as low as  $10^{-4} \text{ yr}^{-1}$  in a disk rotating around a black hole of  $(10^8 - 10^9) M_\odot$  provides a radial flux of angular momentum corresponding to a viscosity parameter  $\alpha \sim 0.1$ .

Collin & Zahn (1999, 2008) built a steady-state accretion disk, including star formation feedback. They argued that the angular momentum redistributed by one SN is lower than the value derived by Różyczka et al. (1995). Therefore, they require a larger number of SN explosions to have the same rate of angular momentum transport. The difference between the prescriptions of Różyczka et al. (1995) and Collin & Zahn (1999, 2008) is related to the uncertainties on the amount of momentum that escapes from the disk carried by the outflowing gas when the SN remnant (SNR) breaks out of the disk.

In the present paper, we reconsider the angular momentum transport in the AGN accretion disks provided by SN explosions. In Section 2, we describe the physical model of the disk. Section 3 gives a general insight into the evolution of SNR in accretion disks around SMBH. In particular, we provide estimates about conditions for the breakout of the disk and give scaling laws for the radial width of the cavity opened by a single SN explosion and the redistribution of angular momentum. In Section 4, we present the results of three-dimensional (3D) simulations, which take into account that some fraction of the mass, energy and momentum can be carried outside the disk by the vertical outflow induced by the explosion. In Section 5, we apply our results to estimate the effective  $\alpha$  viscosity induced by SN explosions. Finally, a summary of the main conclusions is given in Section 6.

## 2. MODEL AND DISK PARAMETERS

We consider an accretion disk in the gravitational field of a central SMBH with mass  $M_{\text{BH}}$  and Schwarzschild radius  $R_{\text{Sch}}$ . In the outer regions of accretion disks, i.e. beyond  $10^3 R_{\text{Sch}}$ , the dust sublimates and the opacity drops. Consequently, these outer regions are expected to be gravitationally unstable and fragmentation of the disk into clouds seems unavoidable (e.g., Goodman 2003; Rafikov 2009; Jiang & Goodman 2011). It is usually assumed that feedback from newly formed stars can maintain the outer parts of accretion disks marginally stable, so that the Toomre  $Q$ -parameter remains close to 1, inhibiting further star formation (e.g., Collin & Zahn 1999; Gammie 2001; Goodman 2003; Sirko & Goodman 2003, hereafter SG; Thompson et al. 2005, hereafter TQM; Rafikov 2009; Begelman & Silk 2017). Radiation pressure from massive stars and from the accretion of gas

onto stellar black holes in the disk, momentum injection from SN explosions, thermal pressure as well as magnetic fields can provide the support necessary to maintain  $Q \simeq 1$ .

There is a wide variety of plausible theoretical models to describe the structure of quasi-stationary self-gravitating accretion disks. They differ on the assumed speed of the radial inflow, the adopted disk opacities and on the importance of the magnetic support. For instance, in the SG model, accretion is driven by local turbulent viscosity, which is parametrized by the Shakura-Sunyaev viscosity parameter  $\alpha$ . TQM presume that a global torque could be able to drive a larger inflow speed than local viscosity. As a result, at distances from the SMBH between  $10^3 R_{\text{Sch}}$  and  $10^5 R_{\text{Sch}}$ , the disk surface density and thickness are smaller in the TQM model than they are in the SG model (a comparison between the outcomes of these models is given in Figure 1 in Bellovary et al. (2016), assuming plausible parameters). Other models suggest that magnetic fields play an important role on the gas dynamics. For example, in magnetically elevated disks, the inflow, which is carried by low-density gas at large heights, is driven mainly by stress due to the large-scale component of the magnetic field (Mishra et al. 2020).

The angular momentum transport due to local turbulence by magnetorotational instabilities (MRI) and gravitational instabilities (GI) can be accommodated in the  $\alpha$  model. The effect of SN explosions on the disk can also contribute to enhance the effective viscosity, which can be also described by a viscosity parameter  $\alpha_{\text{SNe}}$ . The  $\alpha$  parameter will be the sum of all the above contributions:

$$\alpha = \alpha_{\text{MRI}} + \alpha_{\text{GI}} + \alpha_{\text{SNe}} + \alpha_{\text{others}}, \quad (1)$$

where  $\alpha_{\text{others}}$  represent the viscosity due to other potential sources, e.g., star-disk collisions (Pariev et al. 2003). The viscosity coefficients in the right hand side of Eq. (1) are not independent. In the present work, we estimate the contribution of SN explosions to the angular momentum transport, i.e.  $\alpha_{\text{SNe}}$ , in a disk model where the local viscosity  $\alpha$  drives the inflow. Self-consistent models require  $\alpha_{\text{SNe}} \lesssim \alpha$ . In those models where  $\alpha_{\text{SNe}} \sim \alpha$ , SN explosions by themselves can account for the rate of angular momentum transfer.

In the SG model, accretion is driven by local viscosity. In this model, the inflow mass rate  $\dot{M}_{\text{acc}}$  is constant with radius and assumed to be  $l_{\text{Edd}} L_{\text{Edd}} / (\eta c^2)$ , where  $l_{\text{Edd}}$  is the Eddington ratio and  $\eta$  the radiative efficiency. In terms of the dimensionless parameters  $\alpha_{0.1} = \alpha/0.1$  and  $\xi = l_{\text{Edd}} / (\alpha_{0.1} \eta_{0.1})$ , it can be written as

$$\dot{M}_{\text{acc}} = 2.2 \alpha_{0.1} \xi M_8 M_\odot \text{yr}^{-1}, \quad (2)$$

where  $M_8 = M_{\text{BH}} / (10^8 M_\odot)$ . Typical ranges for the values of these parameters are:  $l_{\text{Edd}} = 0.1 - 0.5$ ,  $\eta_{0.1} \simeq 1$  and  $\alpha_{0.1} = 0.1 - 3$ .

Between a radius  $\sim 10^3 R_{\text{Sch}}$  and the outer radius  $10^5 R_{\text{Sch}}$ , Equation (2) together with the condition  $Q = Q_{\text{m}}$  (where  $Q_{\text{m}} \simeq 1$ ) determine the surface density  $\Sigma(R)$ , the scale height  $H(R)$ , the midplane total pressure  $p_0(R)$  and the effective sound speed  $c_s(R)$  (including thermal, radiation and turbulent pressure). More specifically, the Toomre parameter in a Keplerian disk can be expressed

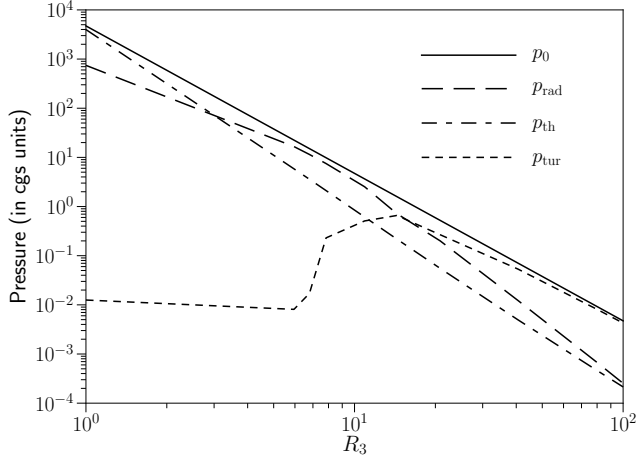


FIG. 1.— Radial profile for the different components of pressure in a model with  $M_8 = 1$ ,  $\alpha_{0.1} = 1$ ,  $\xi = 0.3$  and  $Q_m = 1$ .

as:

$$Q = \frac{H\Omega^2}{\pi G\Sigma} = \frac{\Omega^2}{\sqrt{2\pi^3}G\rho_0}, \quad (3)$$

where  $\Omega(R)$  is the angular velocity of the disk. Note that in the second equality of Equation (3), we have used that the midplane density in a vertically isothermal disk is  $\rho_0 = \Sigma/(\sqrt{2\pi}H)$ . The condition  $Q \simeq Q_m$  implies  $H = \pi Q_m G\Sigma/\Omega^2$ ,  $c_s = \Omega H = \pi Q_m G\Sigma/\Omega$  and

$$\rho_0 = \frac{\Omega^2}{\sqrt{2\pi^3}Q_m G}. \quad (4)$$

The midplane total pressure is  $p_0 = \rho_0 c_s^2 = \sqrt{\pi/2}Q_m G\Sigma^2$ .

By imposing the inflow mass rate given in Equation (2), the SG model predicts

$$\Sigma(R) = 1.6 \times 10^9 \xi^{1/3} Q_m^{-2/3} M_8^{-2/3} R_3^{-3/2} M_\odot \text{pc}^{-2}, \quad (5)$$

$$H(R) = 4.6 \times 10^{-5} \xi^{1/3} Q_m^{1/3} M_8^{4/3} R_3^{3/2} \text{pc}, \quad (6)$$

and

$$c_s = 32 \xi^{1/3} Q_m^{1/3} M_8^{1/3} \text{km s}^{-1}, \quad (7)$$

where  $R_3 = R/(10^3 R_{\text{Sch}})$ . The aspect ratio of the disk  $h(R) \equiv H/R$  is

$$h(R) = 4.6 \times 10^{-3} \xi^{1/3} Q_m^{1/3} M_8^{1/3} R_3^{1/2}. \quad (8)$$

For  $Q_m = 1$ ,  $M_8 = 1$  and  $\xi = 0.3$ , the disk is very thin, with an aspect ratio  $h = 3.1 \times 10^{-3}$  at  $R_3 = 1$ . If we take  $\xi = 5$  as in SG,  $h = 8 \times 10^{-3}$  at  $R_3 = 1$ , in agreement with the value plotted in Figure 2 in SG. These values for the aspect ratio are intermediate between those found in the TQM model ( $h \sim 10^{-3}$ , at  $R_3 \sim 1$ ) and those in magnetically elevated disks ( $h \sim 0.05$ , Mishra et al. 2020).

The scale height given in Equation (6) includes all the components that provide support to the disk: the thermal pressure ( $p_{\text{th}}$ ), the radiation pressure ( $p_{\text{rad}}$ ) and the

turbulent pressure<sup>4</sup> ( $p_{\text{tur}}$ ). The latter is thought to be mostly produced by random motions in the gas excited by SN explosions and stellar winds. Following TQM (see Appendix A for details), we have computed the different contributions ( $p_{\text{th}}$ ,  $p_{\text{rad}}$  and  $p_{\text{tur}}$ ) to the total pressure. The approach of TQM rests on the assumption that star formation is the main feedback mechanism. In that scenario, the radiation-to-turbulent pressure ratio is  $\simeq \tau/2$ , where  $\tau$  is the midplane optical depth. Figure 1 shows the pressure distribution in a disk with  $Q_m = 1$ ,  $\alpha_{0.1} = 1$ ,  $\xi = 0.3$  and  $M_8 = 1$ . We see that the inner region ( $R_3 \lesssim 2.5$ ) is dominated by thermal pressure, an intermediate region dominated by radiation pressure ( $2.5 \lesssim R_3 \lesssim 15$ ), and a region dominated by turbulent pressure at  $15 \lesssim R_3 \lesssim 100$ .

As noted by TQM, a potential problem of disk models driven by a local viscosity is that the star formation rate is so large that it consumes almost all the gas, and little gas is left to fuel the central BH (see also §5.2). However, there are many uncertainties regarding the feedback. In a scenario where irradiation of the disk can also occur from the accretion of gas onto intermediate-mass black holes embedded in the disk (Dittmann & Miller 2020), the ratio between radiation to turbulent pressure could be much larger than  $\tau/2$ . The SG disk is considered a plausible model and has been adopted to study the migration of stellar-mass black holes within AGN disks (McKernan et al. 2012; Bellovary et al. 2016; Secunda et al. 2019; Yang et al. 2020).

Throughout this paper we will make discussions using the SG model (Eqs. 6-7). But since we provide analytical formulae for calculating the impact of SN explosions on the disk, the interested reader can apply them to other disk models.

### 3. SN IN AGN ACCRETION DISKS: EVOLUTION OF A SINGLE EXPLOSION

For simplicity, we consider the evolution of a SN that explodes in the midplane of the accretion disk, at a radial distance  $R_{\text{SNe}}$  from the SMBH, in the range  $10^3 R_{\text{Sch}} \leq R_{\text{SNe}} \leq 10^5 R_{\text{Sch}}$ . The explosion has an energy  $E_{\text{SNe}}$  and a mass ejecta  $M_{\text{SNe}}$ . The momentum associated to this energy and mass is  $P_{\text{SNe}} = (2M_{\text{SNe}}E_{\text{SNe}})^{1/2}$ . The SN explosion will drive a shock in the disk and will carve a cavity of low-density gas, surrounded by a shell of swept material. As a first approach to the evolution of a SN explosion in the disk, we do not include the physics of radiation pressure, radiative transport and self-gravity. Although our hydrodynamical approach is clearly simplistic, we believe that it captures much of the physics of interest.

Given that the problem is multidimensional, it is useful to have analytical estimates of the key quantities. In this Section, we make predictions regarding the radial extent of the cavity, and the redistribution of angular momentum of the disk by a single SN explosion in an initially unperturbed disk with surface density and half thickness as given in Eqs. (5)-(6). As it will become clear in §5, we need these quantities to characterize the contribution of SN explosions to the effective viscosity coefficient.

<sup>4</sup> In the ongoing discussion, we are not considering magnetic fields.

### 3.1. First stage: free expansion phase

An initial free expansion phase will take place until a mass comparable to the SN ejecta has been swept up. Let  $\Delta$  denote the radius of a cylinder perpendicular to the disk at the position  $R_{\text{SNe}}$  that contains a mass  $M_{\text{SNe}}$ . By its definition  $\Delta^2 \equiv M_{\text{SNe}}/(\pi\tilde{\Sigma})$ , where the tilde over a quantity indicates evaluation at  $R_{\text{SNe}}$ , i.e.  $\tilde{\Sigma} \equiv \Sigma(R_{\text{SNe}})$ . In terms of  $\tilde{H}$ , it is

$$\frac{\Delta}{\tilde{H}} = \xi^{-1/2} M_8^{-1} \hat{M}_{10}^{1/2} \tilde{R}_3^{-3/4}, \quad (9)$$

where  $\tilde{R}_3 = R_{\text{SNe}}/(10^3 R_{\text{Sch}})$  and  $\hat{M}_{10} = M_{\text{SNe}}/(10 M_\odot)$ . Thus, for

$$\tilde{R}_3 > \xi^{-2/3} M_8^{-4/3} \hat{M}_{10}^{2/3}, \quad (10)$$

we have  $\Delta \lesssim \tilde{H}$ . This condition implies that when the SNR has a radius  $\sim \tilde{H}$ , the SNR has swept an amount of matter comparable to or larger than the SN ejecta. In particular, for  $M_8 \geq 1$ ,  $\hat{M}_{10} = 1$  and  $\xi = 0.3$ , this condition is met if the SN explosion occurs at a radius  $\tilde{R}_3$  larger than 2.2.

In order to make the presentation clearer, we will consider in the next Sections 3.2 and 3.3 only situations in which  $\Delta \lesssim \tilde{H}$ . The case  $\Delta > \tilde{H}$  is presented in the Appendix B.

### 3.2. Conditions for breakout of the disk

A fraction of the momentum and energy released by the SN vent into the corona if the SNR can breakout of the disk. In this subsection we consider the conditions in which breakout of the disk occurs. For simplicity, we will implicitly assume that  $\Delta$  is significantly smaller than  $\tilde{H}$ .

Kompaneets (1960) studied the propagation of the shock wave in a plane-parallel stratified medium. It was shown that if the explosion occurs at the midplane, the SNR is prolate in shape because the expansion velocity of the shell will be higher in the vertical direction than in the radial direction. Let denote  $Z_{\text{sh}}(t)$  the vertical distance of the topmost point of the shell (i.e., the semi-major axis in the  $z$ -direction of the prolate SNR) and  $R_{\text{sh}}(t)$  the radius of the SNR in the  $z = 0$  plane.  $\dot{Z}_{\text{sh}}$  decreases with  $z$  up to a certain height  $z_b$ , and then it is reaccelerated (e.g., Kompaneets 1960; Mac Low, McGray & Norman 1989; Ferrara & Tolstoy 2000). The SN explosion will break out of the disk if  $v_b > \tilde{c}_s$  where  $v_b$  is the velocity of the shock  $\dot{Z}_{\text{sh}}$  at  $z_b$  (e.g., Ferrara & Tolstoy 2000).

In order to calculate  $v_b$ , we consider two limiting scenarios. In scenario A, we assume that the SNR reaches the reaccelerating height  $z_b$  with negligible radiative cooling. Thus, we may use the Kompaneets approximation to evaluate the  $z$ -component of the velocity of the topmost point of the shell as  $\dot{Z}_{\text{sh}}(z) \simeq [E_{\text{SNe}}/(\tilde{\rho} z^3)]^{1/2}$ , where  $\tilde{\rho}(z) = \tilde{\rho}_0 \exp(-z^2/[2\tilde{H}^2])$  (e.g., Ferrara & Tolstoy 2000; Olano 2009). Scenario B assumes that cooling is already important at the end of the free expansion phase so that the pressure interior to the shell is negligible. In such a case, momentum-conservation implies  $\dot{Z}_{\text{sh}}(z) \simeq 3P_{\text{SNe}}/(4\pi\tilde{\rho} z^3)$ , again if  $Z_{\text{sh}} < z_b$ . Other possibilities that may be considered more realistic, as a

pressure modified snowplow phase, lie between these two limiting scenarios.

Assuming that the disk has a vertical Gaussian profile, we find  $z_b = \sqrt{3}\tilde{H}$  in both scenarios. In scenario A and for our disk model (Eqs. 5 and 6), we get

$$v_b = 5.5 \times 10^3 \xi^{-1/2} M_8^{-1} E_{51}^{1/2} \tilde{R}_3^{-3/4} \text{ km s}^{-1}, \quad (11)$$

where  $E_{51} = E_{\text{SNe}}/(10^{51} \text{ erg})$ . The breakout condition  $v_b > \tilde{c}_s$  implies that SNR can punch a hole in the disk if the explosion occurs within a radius  $\tilde{R}_b^{(A)}$  given by

$$\tilde{R}_3 \leq \tilde{R}_b^{(A)} \equiv 1.0 \times 10^3 \xi^{-10/9} M_8^{-14/9} E_{51}^{2/3}. \quad (12)$$

For the reference values  $\xi = 0.3$  and  $E_{51} = 1$ , we find that  $\tilde{R}_b^{(A)} \gtrsim 20$ , if  $M_8 \leq 30$ . In particular, for  $M_8 = 1$ , we obtain that  $\tilde{R}_b^{(A)} = 3.8 \times 10^3$ , which is much larger than the outer edge of the accretion disk.

In scenario B, we get

$$v_b \simeq 4.5 \times 10^3 \xi^{-1} M_8^{-2} \hat{M}_{10}^{1/2} E_{51}^{1/2} \tilde{R}_3^{-3/2} \text{ km s}^{-1}. \quad (13)$$

The breakout condition is fulfilled if

$$\tilde{R}_3 \leq \tilde{R}_b^{(B)} \equiv 30 \xi^{-8/9} M_8^{-14/9} \hat{M}_{10}^{1/3} E_{51}^{1/3}. \quad (14)$$

For  $\xi = 0.3$  and  $M_8 = 1$ , a SN explosion with  $E_{51} = \hat{M}_{10} = 1$  is capable to break out of the disk in the range of interest  $1 \leq \tilde{R}_3 \leq 100$ . On the contrary, if  $M_8 \geq 18$ , SN explosions with  $E_{51} = \hat{M}_{10} = 1$  will never breakout of the disk at  $\tilde{R}_3 > 1$ .

### 3.3. Radial width of the SNR

In the  $z = 0$  plane, the otherwise circular SNR will be deformed by the Coriolis forces in a first stage, when the expansion velocity of the SNR  $\dot{R}_{\text{sh}}$  is still much larger than the shear velocity. In a second stage, when  $\dot{R}_{\text{sh}}$  becomes comparable to the shear velocity, the SNR will become elongated along the azimuthal direction, resembling an ellipse in shape, due mainly to differential rotation induced by the ram pressure with the ambient medium (Olano 1982; Tenorio-Tagle & Palous 1987; Palous, Franco, & Tenorio-Tagle 1990; Silich 1992; Różyczka et al. 1995). In a final stage, shear dominates and the radial width of the cavity  $W$  may decrease over time (e.g., Tenorio-Tagle & Palous 1987). In this section, we evaluate the maximum radial width of the SNR, denoted by  $W_{\text{max}}$ , in scenario A. An analogue derivation but for scenario B can be found in Appendix C.

Let denote  $W_{\text{max}}^{\text{trans}}$  the width of the SNR when the shock velocity drops to a value similar to the effective sound speed of the external medium (i.e. the shock velocity becomes transonic), and  $W_{\text{max}}^{\text{shear}}$  the radial width of the SNR when the shock velocity is comparable to the shear velocity  $\simeq (3/4)\tilde{\Omega}R_{\text{sh}}$ , where  $\tilde{\Omega}$  is the angular velocity. The maximum width of the SNR will be given by  $W_{\text{max}} = \min[W_{\text{max}}^{\text{trans}}, W_{\text{max}}^{\text{shear}}]$ .

The expansion velocity  $\dot{R}_{\text{sh}}$  of the SNR depends on the thermodynamics of the gas and on the fraction of momentum that is transferred into the disk. In order to compute  $\dot{R}_{\text{sh}}$ , we will consider the adiabatic phase and the momentum-driven snowplow phase. Therefore, we implicitly assume that a mass of gas larger than the SN ejecta has been swept up. As a consequence, our results

are valid only if  $\tilde{\rho}_0 W_{\max}^3 \gtrsim 8M_{\text{SNe}}$ , i.e.  $W_{\max} > W_{\text{lim}} \equiv 2(M_{\text{SNe}}/\tilde{\rho}_0)^{1/3}$ .

Consider first the case where the SN explosion occurs at a distance  $\tilde{R}_3 < \tilde{R}_b^{(A)}$  from the SMBH. If so, the SN can make a hole in the disk. At short times after the explosion, before breakout of the disk, when  $R_{\text{sh}}^2 + Z_{\text{sh}}^2 \ll \tilde{H}^2$ , the shell is spherical because the SNR evolves as if the medium were homogeneous, so that  $\dot{R}_{\text{sh}} = \dot{Z}_{\text{sh}} \simeq (2/5)(E_{\text{SNe}}/[\tilde{\rho}_0 R_{\text{sh}}^3])^{1/2}$ . The interior pressure of the SNR continue pushing the shell in both the vertical and radial directions while the SNR is embedded within the disk, i.e. while  $R_{\text{sh}} \sim Z_{\text{sh}} \lesssim \tilde{H}$ . At some point, the flow accelerates in the vertical direction leading to a rapid depressurization of the cavity. This phase of depressurization starts when  $R_{\text{sh}} \simeq \tilde{H}$  and  $Z_{\text{sh}} \simeq \sqrt{3}\tilde{H}$  (see §3.2). We recall here that  $\tilde{H}$  is the scaleheight of the disk prior breakout, which includes the vertical support provided by the turbulent pressure. Anticipating to what we observe in the simulations, the SNR forms an overdense ring-like structure in the disk, with expansion velocity  $\dot{R}_{\text{sh}}$ . If we assume that after depressurization of the cavity, the ring-like SNR enters into a snowplow phase, momentum conservation may be expressed as

$$R_{\text{sh}}^2 \dot{R}_{\text{sh}} \simeq \chi_A \tilde{H}^2 \dot{R}_{\text{sh}}(\tilde{H}), \quad (15)$$

where  $\chi_A$  is a dimensionless correction factor to account for the push by the interior pressure during the pressure-driven phase. Equation (15) encapsulates the fact that the interior pressure of the cavity can push the shell for a longer time if the disk (prior to breakout) is thick, imparting more momentum to the shell than in more thin disks (e.g., Tenorio-Tagle & Palous 1987). From the Kompaneets approximation, we have  $\dot{R}_{\text{sh}}(\tilde{H}) \simeq 0.4(E_{\text{SNe}}/[\tilde{\rho}_0 \tilde{H}^3])^{1/2}$ . Using this value in Equation (15), we can derive  $\dot{R}_{\text{sh}}$ . The transonic condition implies

$$W_{\max}^{A,\text{trans}} \simeq 1.2 \left( \frac{\chi_A^2 E_{\text{SNe}} \tilde{H}}{\tilde{\rho}_0 \tilde{c}_s^2} \right)^{1/4}. \quad (16)$$

In our disk model

$$W_{\max}^{A,\text{trans}} \simeq 7.5 \times 10^{-4} \chi_A^{1/2} \xi^{-1/12} Q_{\text{m}}^{1/6} E_{51}^{1/4} M_8^{2/3} \tilde{R}_3^{9/8} \text{ pc}. \quad (17)$$

The condition  $\dot{R}_{\text{sh}} \simeq (3/4)\tilde{\Omega}R_{\text{sh}}$  leads to

$$W_{\max}^{A,\text{shear}} \simeq 1.6 \left( \frac{\chi_A^2 E_{\text{SNe}} \tilde{H}}{\tilde{\rho}_0 \tilde{\Omega}^2} \right)^{1/6}. \quad (18)$$

The dependence of  $W_{\max}^{A,\text{shear}}$  on  $E_{\text{SNe}}$ ,  $\tilde{\rho}_0$  and  $\tilde{H}$  is weak. This agrees with the fitting formula found in Palous, Franco, & Tenorio-Tagle (1990) for the SNR minor axis in the  $z = 0$  plane. Using a model in 1.5 dimensions that describes the propagation of the shell from a strong explosion in a rotating disk, they found that the semiminor axis is proportional to  $E_{\text{SNe}}^{0.22} \tilde{\rho}_0^{-0.22} \tilde{H}^{0.1}$  (their Equation 4). In terms of our independent variables and for our disk model, Equation (18) becomes

$$W_{\max}^{A,\text{shear}} \simeq 4 \times 10^{-4} \chi_A^{1/3} \xi^{1/18} Q_{\text{m}}^{2/9} M_8^{8/9} E_{51}^{1/6} \tilde{R}_3^{5/4} \text{ pc}. \quad (19)$$

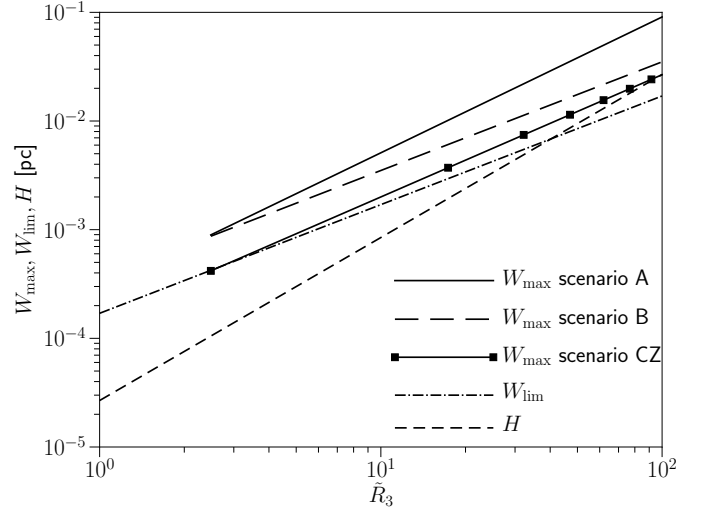


FIG. 2.—  $W_{\max}$  as a function of radius for a model with  $M_8 = 1$  in scenario A (solid line), in scenario B (long dashed line) and using Eq. (24) (solid line with small squares). We take  $\xi = 0.3$ ,  $Q_{\text{m}} = 1$ ,  $E_{51} = 1$  and  $\chi_A = \chi_B = 1$ . The scale height of the disk  $H$ , and  $W_{\text{lim}} \equiv 2(M_{\text{SNe}}/\tilde{\rho}_0)^{1/3}$  are also shown. For this range of parameters, the SNR breaks out of the disk.

If the explosion occurs at  $\tilde{R}_3 > \tilde{R}_b^{(A)}$ , the disk is not perforated. Thus, the shell is confined to the disk. When the explosion occurs at the midplane, Kompaneets's approximation implies that  $\dot{R}_{\text{sh}} \simeq 0.4(E_{\text{SNe}}/[\tilde{\rho}_0 R_{\text{sh}}^3])^{1/2}$  if  $Z_{\text{sh}} \leq z_b = \sqrt{3}\tilde{H}$  (see Fig. 2 in Olano 2009). The transonic condition  $\dot{R}_{\text{sh}} \simeq \tilde{c}_s$ , leads to

$$W_{\max}^{A,\text{trans}} \simeq \left( \frac{E_{\text{SNe}}}{\tilde{\rho}_0 \tilde{c}_s^2} \right)^{1/3}. \quad (20)$$

For our accretion disk model (Eqs. 5-7), we can recast  $W_{\max}^{A,\text{trans}}$  in terms of  $M_8$  and  $\tilde{R}_3$  as

$$W_{\max}^{A,\text{trans}} \simeq 1.5 \times 10^{-3} \xi^{-2/9} Q_{\text{m}}^{1/9} E_{51}^{1/3} M_8^{4/9} \tilde{R}_3 \text{ pc}. \quad (21)$$

On other hand, if the radial expansion of the SNR is limited by shear, the condition  $\dot{R}_{\text{sh}} \simeq (3/4)\tilde{\Omega}R_{\text{sh}}$  implies

$$W_{\max}^{A,\text{shear}} \simeq 0.8 \left( \frac{E_{\text{SNe}}}{\tilde{\rho}_0 \tilde{\Omega}^2} \right)^{1/5}. \quad (22)$$

For our disk model,

$$W_{\max}^{A,\text{shear}} \simeq 6 \times 10^{-4} Q_{\text{m}}^{1/5} M_8^{4/5} E_{51}^{1/5} \tilde{R}_3^{6/5} \text{ pc}. \quad (23)$$

The corresponding values of  $W_{\max}$  in scenario B are given in the Appendix C (see Eqs. C9-C10). Figure 2 compares  $W_{\max}$  in scenario A and scenario B, assuming  $Q_{\text{m}} = 1$ ,  $M_8 = 1$  and  $E_{51} = 1$ . The values of the width  $W_{\max}$  are larger than  $\tilde{H}$  because the SNR breakouts of the disk, for the range of values of  $\tilde{R}_3$  under consideration. Since the SNR in scenario B evolves as a pure momentum-driven snowplow, the values of  $W_{\max}^{B,\text{trans}}$  and  $W_{\max}^{B,\text{shear}}$  are smaller than the corresponding values in scenario A. We should note that we have assumed  $\chi_A = \chi_B = 1$  for convenience.

Figure 3 shows the same quantities as Figure 2 but for  $M_8 = 100$ . SNR formed within the range  $10^3 R_{\text{Sch}}$  and

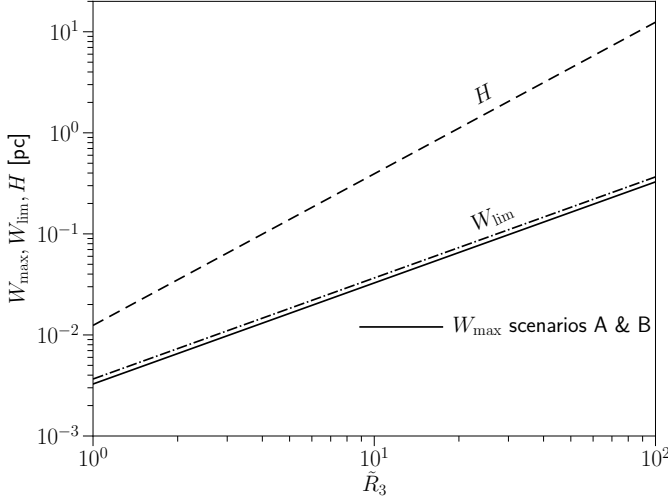


FIG. 3.—  $W_{\max}$  as a function of radius for a model with  $M_8 = 100$  in scenario A and B (solid line). We take  $\xi = 0.3$ ,  $Q_m = 1$  and  $E_{51} = 1$ . The scale height of the disk  $H$  and  $W_{\lim}$  are also shown. For this range of parameters, the SNR is confined to the disk.

$10^5 R_{\text{Sch}}$  and  $E_{51} = 1$ , have not enough energy to break out of the disk. In addition, we see that the curve of  $W_{\max}$  is very close to the curve for  $W_{\lim}$ . This indicates that the values of  $W_{\max}$  should be taken with caution.  $W_{\max}$  in scenarios A and B are similar. In fact, the curves for scenarios A and B overlap.

There has been other attempts to estimate  $W_{\max}$  in the literature. Collin & Zahn (1999) suggest that for SN explosions powerful enough as to produce breakout of the disk, the momentum transferred to the disk is  $P_{\text{SNe}} W_{\max} / (2\tilde{H})$ . As a result, they find

$$W_{\max}^{\text{CZ, shear}} \approx 1.1 \left( \frac{P_{\text{SNe}}}{\pi \tilde{\rho}_0 \tilde{\Omega}} \right)^{1/4}. \quad (24)$$

For the parameters of Figure 2,  $W_{\max}^{\text{CZ, shear}}$  is roughly a factor of 2–3 smaller than  $W_{\max}^{\text{B, shear}}$ . This implies that we would need  $\chi_B \simeq 0.1$  to have a match between both estimates. 3D simulations can shed light on the appropriate value for the fraction of momentum that is absorbed by the disk.

### 3.4. Angular momentum redistribution in the disk by SN explosions

SN explosions may redistribute the angular momentum of the disk. As discussed in Różyczka et al. (1995), disk gas elements that enter the shock facing the inner disk lose angular momentum, whereas gas elements that cross the shock facing the outer disk gain angular momentum. The net effect is a transport of angular momentum radially outwards. Denote  $\mathcal{J}_{\text{SNe}}$  the total amount of angular momentum that is transported from the inner disk to the outer disk by just one SN explosion. Różyczka et al. (1995) show that  $\mathcal{J}_{\text{SNe}}$  is given by

$$\mathcal{J}_{\text{SNe}} = \mu \tilde{\Sigma} \dot{R}_{\text{sh}} R_{\text{sh}}^2 R_{\text{SNe}}, \quad (25)$$

where  $R_{\text{sh}}$  and  $\dot{R}_{\text{sh}}$  should be evaluated once the SNR has breakout of the disk (see Section 4.2 in Różyczka et al.

(1995)). In Equation (25) we have introduced the fudge factor  $\mu$  to be fixed through our numerical simulations in Section 4. This factor may depend on the scenario, so we will refer to them as  $\mu_A$  and  $\mu_B$ .

In scenario A, we can use Eqs. (15) and (25), plus the disk scaling laws in Eqs. (5) and (6) to obtain

$$\mathcal{J}_{\text{SNe}}^{(A)} = 0.6 \beta_A (E_{\text{SNe}} \tilde{\Sigma})^{1/2} \tilde{H} R_{\text{SNe}} = 75 \beta_A \xi^{1/2} E_{51}^{1/2} M_8^2 \tilde{R}_3^{7/4} \quad (26)$$

where  $\beta \equiv \mu \chi$  and  $\mathcal{J}_{\text{SNe}}^{(A)}$  is in units of  $M_{\odot} \text{pc km/s}$ .

In scenario B, momentum conservation implies  $\dot{R}_{\text{sh}} R_{\text{sh}}^2 = \beta_B P_{\text{SNe}} / (\pi \tilde{\Sigma})$  (see Eq. C6). Thereby, we find

$$\mathcal{J}_{\text{SNe}}^{(B)} = \frac{\beta_B}{\pi} P_{\text{SNe}} R_{\text{SNe}} = 100 \beta_B M_8 \hat{M}_{10}^{1/2} E_{51}^{1/2} \tilde{R}_3, \quad (27)$$

again in units of  $M_{\odot} \text{pc km/s}$ . The next Section is devoted to simulate the 3D evolution of a SNR in a disk and inferences of  $\beta$  will be provided.

## 4. SIMULATIONS

Our 3D simulations of the evolution of a SNR in a disk in Keplerian rotation were performed using the code FARGO3D<sup>5</sup> (Benítez-Llambay & Masset 2016) in a spherical coordinate system  $(r, \theta, \phi)$ . Magnetic fields and self-gravity of the disk were ignored.

We placed the site of the SN explosion at the mid-plane of the disk. Given the symmetry of problem, we simulated only the upper half of the disk. We chose a system of reference that rotates with the angular velocity at  $R_{\text{SNe}}$ , so that the explosion site does not change over time. We took  $M_8 = 1$  and  $\tilde{R}_3 = 20$ , which corresponds to  $R_{\text{SNe}} = 0.2$  pc. In this model, the circular velocity of a test particle with orbital radius  $R_{\text{SNe}}$  is  $1467 \text{ km s}^{-1}$  and its orbital period  $P_{\text{orb}}$  is 838 yr.

The initial surface density is given in Equation (5). At  $R_{\text{SNe}}$ , it is  $1.2 \times 10^7 M_{\odot} \text{pc}^{-2}$ . The initial vertical profile of density was derived by assuming that the temperature of the gas is independent of  $\theta$ , and imposing hydrostatic equilibrium with an aspect ratio  $h = 0.01375 (R/R_{\text{SNe}})^{1/2}$ . Thus the isothermal sound speed is  $21.4 \text{ km s}^{-1}$ , constant along the disk.

The mass ejecta is  $M_{\text{SNe}} = 10 M_{\odot}$  and the explosion has an energy  $E_{\text{SNe}} = 2 \times 10^{51} \text{ erg}$ . As we are modeling only one half of the disk, we deposit  $5 M_{\odot}$  and  $10^{51} \text{ erg}$  in our domain. At  $t = 0$ , this mass and energy is injected by increasing the density and the thermal energy of the gas into a region with a radius of  $6.5 \times 10^{-5} \text{ pc}$ . The equation of energy is solved by assuming the equation of ideal gas  $p = (\gamma - 1)e$  where  $p$  is the gas pressure and  $e$  the internal energy density. For the adiabatic index, we take  $\gamma = 5/3$  (model 1) and  $\gamma = 1.1$  (model 2).

The azimuthal angle ranges from 0 to  $\pi/2$ . Hence, we only simulate an octant of the disk. The explosion center is placed at  $\phi = \pi/4$ . The latitude,  $\pi/2 - \theta$ , ranges from 0 (midplane of the disk) to  $6.2\tilde{h}$  (in radians), where  $\tilde{h}$  is the aspect ratio of the disk at the explosion center. In the radial direction, the domain extends from  $r_{\text{in}} = 0.15 \text{ pc}$  to  $r_{\text{out}} = 0.25 \text{ pc}$ . In the upper tap of the disk we employ open boundary conditions. Damping boundary conditions for the radial component of the velocity has been used at  $r_{\text{in}}$  and at  $r_{\text{out}}$  (de Val-Borro et al. 2006).

<sup>5</sup> The code is publicly available at <http://fargo.in2p3.fr>

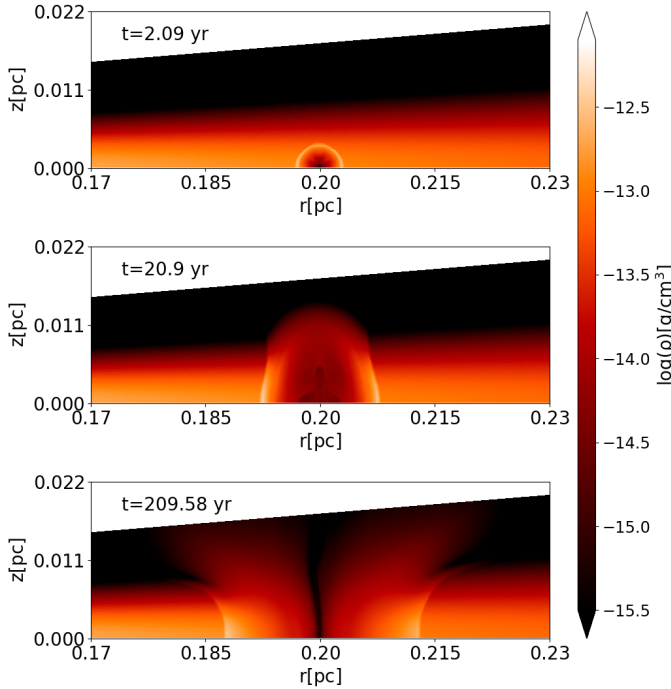


FIG. 4.— Vertical cut of the gas density along the radial direction, passing through the SN explosion site ( $\phi = \pi/4$ ), in model 1.

The number of zones in each direction are  $N_r = 768$ ,  $N_\theta = 128$  and  $N_\phi = 2304$ .

#### 4.1. Evolution of the SNR

We will first focus on model 1. Model 2 will be discussed at the end of this Section. Since model 1 is adiabatic with  $\gamma = 5/3$ , we will use scenario A, which ignores cooling, to make predictions.

For the parameters in model 1, the condition for breakout of the disk (Equation 12) is satisfied. Figure 4 shows vertical cuts of the volume density along the radial direction, passing through the explosion center, in model 1. At  $t = 20.9$  yr, the disk is in the process of breakout; the blast wave in the  $z$ -direction is just leaving the disk. The shape of the SNR in this vertical plane is prolate ( $R_{\text{sh}} = 2.7\tilde{H}$  and  $Z_{\text{sh}} = 4.85\tilde{H}$ , at  $t = 20.9$  yr) because the  $z$ -direction presents less resistance. Before the breakout of the disk, the shell in these cuts appears as convex arcs, but after breakout these arcs become concave. Some of the vented gas escapes from our computational domain. Before presenting a more quantitative analysis of the mass lost through the boundaries of our computational domain, we will look at the evolution of the SNR along different cuts.

The evolution of the volume density in the midplane of the disk is shown in Figure 5. The gas disk rotates counterclockwise. At  $t \leq 20$  yr, the SNR along a cut through the  $z = 0$  plane is almost circular, though a bit elongated due to the Coriolis force. At  $t = 41.91$  yr, the SNR has an ellipsoidal shape with axis ratio  $\sim 0.72$ . The angle between the major axis of the ellipse and the radial direction is  $\simeq 45^\circ$ . Due to the differential rotation of the accretion disk, the shear continues

stretching the SNR in the azimuthal direction (see panel at  $t = 209.58$  yr). At this time, the SNR presents a banana-like shape. Between  $t = 209.6$  yr ( $0.25P_{\text{orb}}$ ) and  $t = 335.3$  yr ( $0.4P_{\text{orb}}$ ), the major axis of the SNR continues growing, while its minor axis (width along the radial direction) barely changes.

The overall evolution of the shape of the SNR in the disk midplane is similar to that described in Tenorio-Tagle & Palous (1987) in the context of formation of holes in galactic H I disks by the explosion of multiple SN in evolved OB associations. In such a study, they used a 1.5-dimensional model of the SNR and assumed a flat rotation curve (see also Palous, Franco, & Tenorio-Tagle 1990). The morphology of the SNR is also similar to the results in Różyczka et al. (1995), who made 2D simulations of a SN explosion in a Keplerian disk.

To gain a more physical insight to the evolution of the SNR, Figure 6 shows the volume gas density at the midplane of the disk along a radial cut that passes through the explosion center, i.e. for  $\phi = \pi/4$ . As expected, at the very center of the SNR, the material has been evacuated efficiently. The maximum radial width of the SNR is  $W_{\text{max}} = 0.026$  pc or, in terms of the local scale height  $W_{\text{max}} = 9.5\tilde{H}$ . Between 10.2 yr and 83.8 yr, the peaks in density, which correspond to the position of the shell, are equally spaced, implying an effective radial expansion velocity in  $\text{km s}^{-1}$

$$\dot{W} = 5 \times 10^3 \exp\left(-\frac{W}{0.005}\right), \quad (28)$$

where  $W$  is in pc. The effective velocity  $\dot{W}/2$  is supersonic at  $t \leq 100$  yr. We also see that during the first 100 yr after the explosion, the SNR is able to keep the cavity clean of material, indicating that the SNR is able to deflect the disk gas entering the SNR.

After  $t \simeq 100$  yr, the behaviour of the SNR changes.  $W$  increases very slowly, so that the expansion of the SNR in the radial direction has almost stalled at  $t = 167$  yr (see Figure 6). After  $t = 167$  yr, the density in the cavity starts to increase. The reason is that the disk gas can penetrate into the cavity. In fact, as time goes on, the shock waves weaken and the pitch angle decreases. As a result, the deflection of the disk gas that enters the SNR is much more moderate. The elements inside the cavity are accelerated inward due to the pressure gradient that tries to refill the cavity (see Figure 7). Indeed, after 100 yr, the central cavity is depressurized and the evolution follows a momentum-conservation phase. The disk velocity field at 335.3 yr after the explosion is shown in Figure 8. In this “passive” phase, the SNR only grows along the azimuthal direction.

Since our simulations are 3D, we have information about the redistribution of mass in the vertical direction, and on the amount of mass that is vented into the corona. Figure 9 shows the mass that has been lost from our computational domain at a given time. The mass loss rate is approximately constant between  $t = 40$  yr and  $t = 170$  yr. Mass expulsion from our domain is halted at 200 yr after the explosion. Approximately a mass of  $300M_\odot$  is lost through the upper boundary.

Now consider the mass that is contained below a height of  $3H$  from the midplane, i.e. at  $z < 3H$  (see also Figure 9). We see that the SN explosion is cleaning up mate-

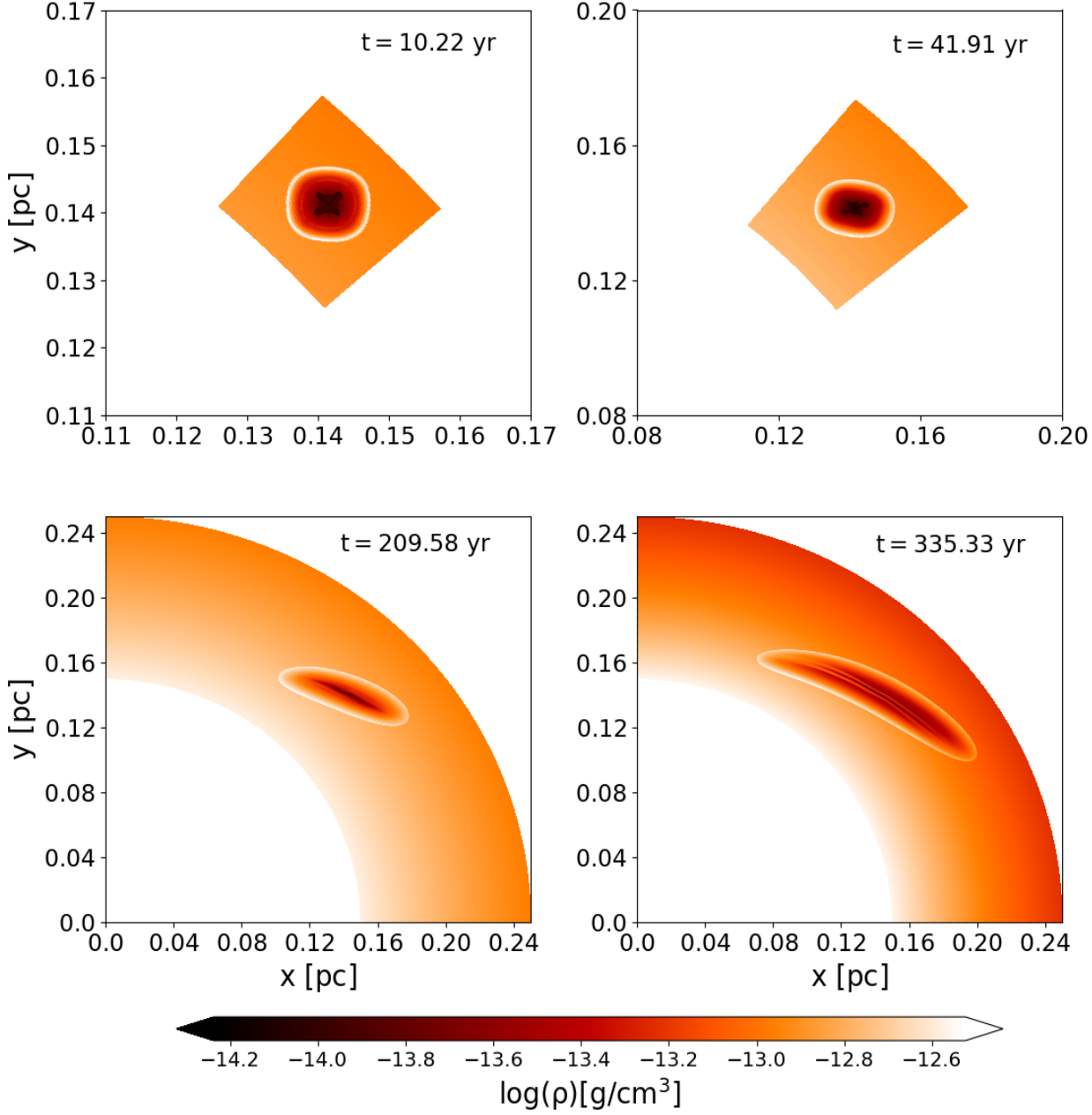


FIG. 5.— Volume density at the midplane ( $z = 0$ ) in model 1, at four different times.

rial from  $z < 3H$  during the first  $\sim 250$  yr after the explosion. It is interesting to note that a significant fraction of the mass that has been evacuated from regions  $z < 3H$  remains in the region  $3H < z < 6.2H$ . For instance, at  $t = 250$  yr, the mass evacuated from  $z < 3H$  is  $\sim 1000M_{\odot}$  and 70% of this mass remains at altitudes between  $3H$  and  $6.2H$ . Figure 10 illustrates how the azimuthally-averaged volume density,  $\langle \rho \rangle_{\phi}$ , is distributed in the upper parts in the model 1 at two different times.

The velocity of expansion of the SNR depends on the adopted adiabatic index  $\gamma$ . The smaller the value of  $\gamma$ , the lower the internal pressure that pushes outward on the shell. Because cooling in the accretion disk is efficient, values of  $\gamma$  close to 1 are thought to be more

realistic. In order to quantify the dependence of the flow pattern on the adiabatic index, we carried out a simulation with the same parameters as model 1, but using  $\gamma = 1.1$  (model 2).

Figure 11 shows cuts of the density through the center of the SN explosion along the radial direction in model 2, whereas Figure 12 shows cuts of the pressure along the azimuthal direction. The SNR acquires a maximum width along the radial direction of  $W_{\max} \simeq 0.02$  pc, which is a factor of 1.3 smaller than in model 1. The expansion velocity of the SNR in the azimuthal direction is also slower than in model 1. The amount of mass that is carried outside the region  $z < 3H$  by the SNR is a factor of  $\sim 3$  smaller in model 2 than it is in model 1 (see

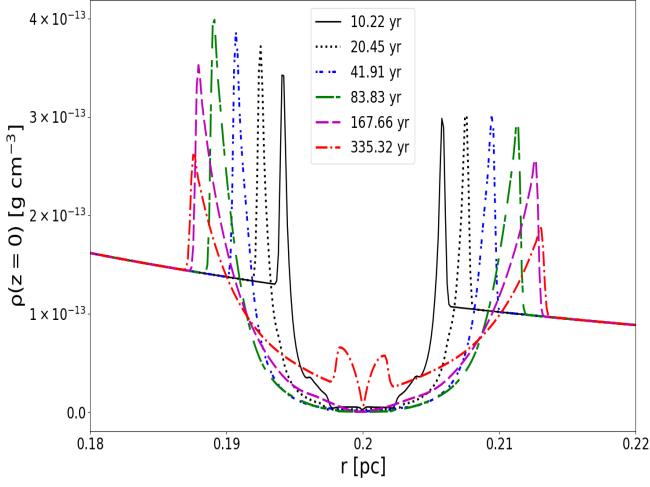


FIG. 6.— Volume density at the midplane of the disk as a function of radius  $r$ , in the direction of the explosion center ( $\phi = \pi/4$ ), at different times, in model 1.

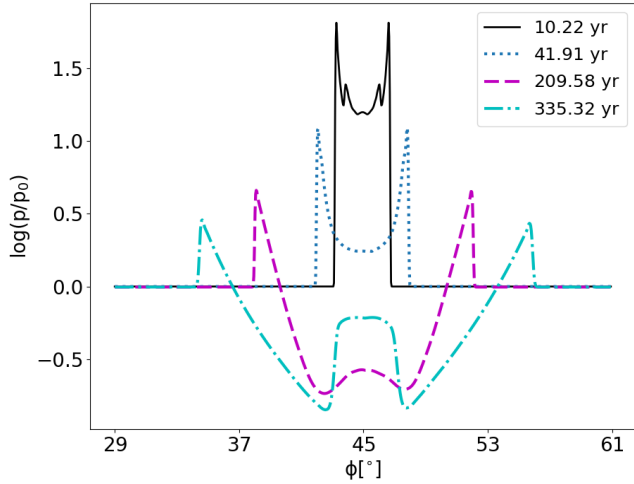


FIG. 7.— Cross sections of the gas pressure along the azimuthal direction at  $z = 0$  and  $R = R_{\text{SNe}}$  in model 1.  $p_0$  is the unperturbed pressure. Note that  $6^\circ$  are 0.021 pc.

Figure 13). Likewise, the mass that escapes from the computational domain is a factor of 3 smaller in model 2 than in model 1. In the next subsection, we will compare the amount of angular momentum that is redistributed by the SNR in models 1 and 2.

#### 4.2. Determining $\chi$ and $\beta$

In Sections 3.3 and 3.4, we have introduced some dimensionless factors when deriving the scaling laws that obey  $W_{\text{max}}$  and  $\mathcal{J}_{\text{SNe}}$  from theoretical grounds. These factors, which are expected to be of the order of unity, can be measured in our simulations.

We have computed  $\chi_A$  in our simulations as follows. From Equation (15), the momentum imparted to the disk  $\pi \tilde{\Sigma} R_{\text{sh}}^2 \dot{R}_{\text{sh}}$  is  $0.4 \pi \chi_A \tilde{\Sigma} \tilde{H}^2 (E_{\text{SNe}} / \tilde{\rho}_0 \tilde{H}^3)^{1/2} = 2 \chi_A \tilde{H} (E_{\text{SNe}} \tilde{\Sigma})^{1/2}$ . Therefore, we can measure  $\chi_A$  in our

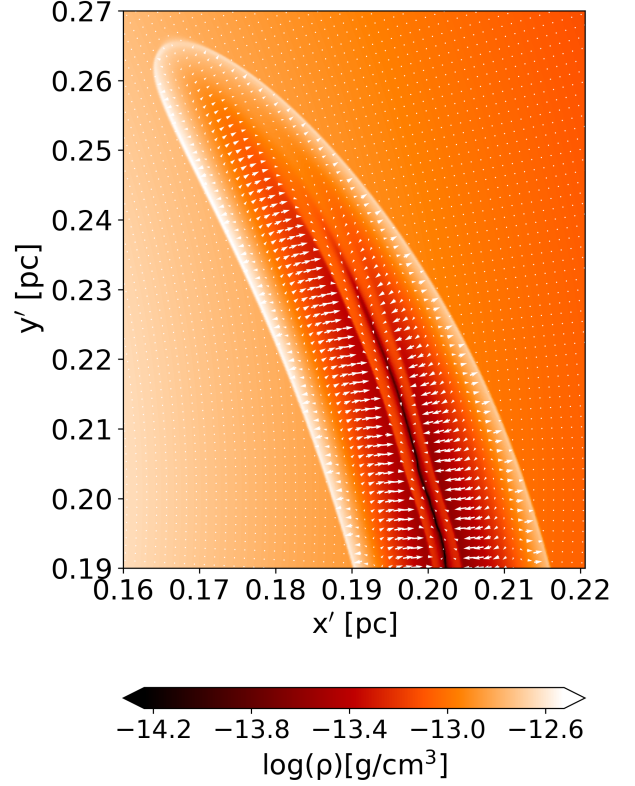


FIG. 8.— Color map of the volume density overlaid with the perturbed velocity field (after subtracting the Keplerian velocity field) at  $z = 0$  and  $t = 335.3$  yr in model 1.

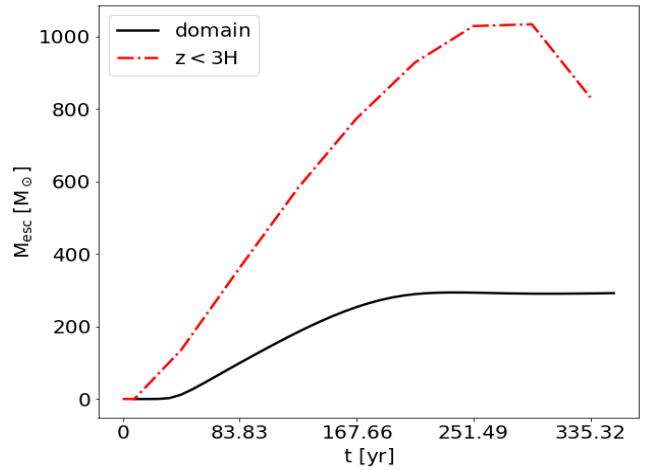


FIG. 9.— Mass that has escaped from our computational domain (solid line) and the mass that has exited the region  $z < 3H$  (dashed line), in model 1.

simulations as

$$\chi_A \simeq \frac{1}{\tilde{H} (E_{\text{SNe}} \tilde{\Sigma})^{1/2}} \int_{z < 3H} \rho \delta v_{\parallel} d^3 \mathbf{r}, \quad (29)$$

where  $\delta v_{\parallel} = \sqrt{\delta v_x^2 + \delta v_y^2}$  is the planar component of the perturbed velocity field  $\delta \mathbf{v} = \mathbf{v} - \mathbf{v}_0$ , with  $\mathbf{v}_0$  is the un-

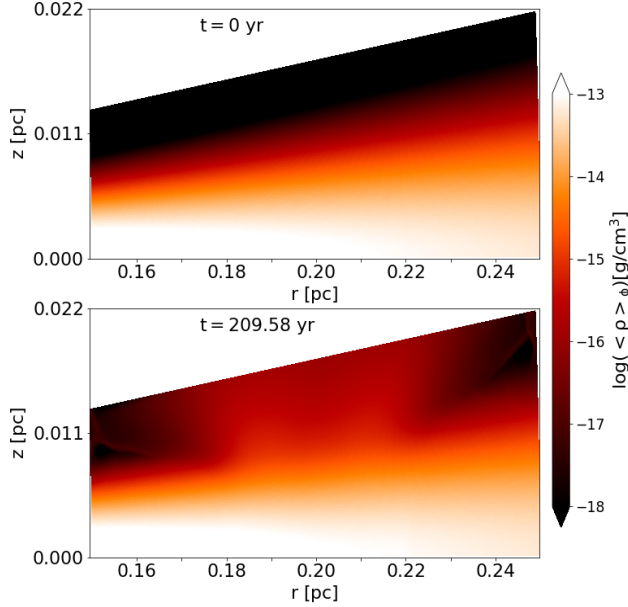


FIG. 10.— Azimuthally-averaged volume density in model 1 at  $t = 0$  (top) and at  $t = 209.58$  yr (bottom).

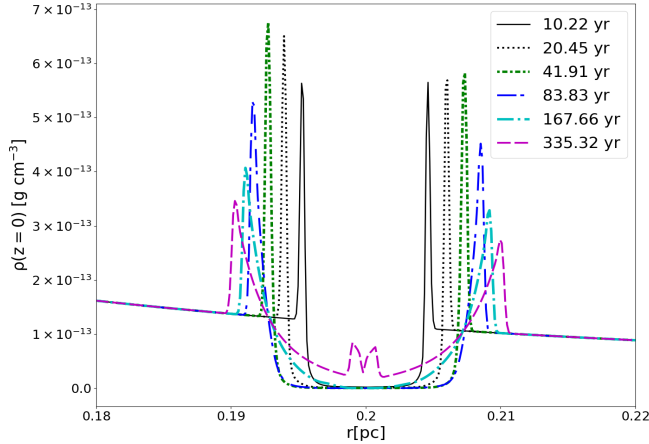


FIG. 11.— Midplane density along a radial cut under  $\phi = \pi/4$ , in model 2 ( $\gamma = 1.1$ ).

perturbed Keplerian velocity of the disk. In model 1, we have computed  $\chi_A$  at  $t = 41.9$  yr, when the low-density cavity produced by the explosion is still circular in the  $z = 0$  plane (see Figure 5), and at  $t = 83.8$  yr, when the SNR has evacuated a significant mass of the disk. We find  $\chi_A \simeq 0.7$  at both times.

Once we know  $\chi_A$ , we can evaluate the predicted maximum width of the SNR in scenario A as described in Section 3.3. From Eqs. (16) and (18) with  $\chi_A = 0.7$ ,  $\xi = 0.3$ ,  $E_{51} = 2$ , we find  $W_{\max}^{A,\text{trans}} = 0.02$  pc and  $W_{\max}^{A,\text{shear}} = 0.011$  pc. The maximum width measured in model 1 is 0.026 pc. Therefore, our  $W_{\max}^{A,\text{shear}}$  underestimates the width by a factor of  $\sim 2$ . Interestingly, for  $\chi_A = 1$ ,  $W_{\max}^{A,\text{trans}} = 0.024$  pc, which is close to the value obtained from our simulations.

A value of  $\chi_A \simeq 0.7$  is probably more adequate for simulations with a lower value of  $\gamma$ . In order to test this idea,

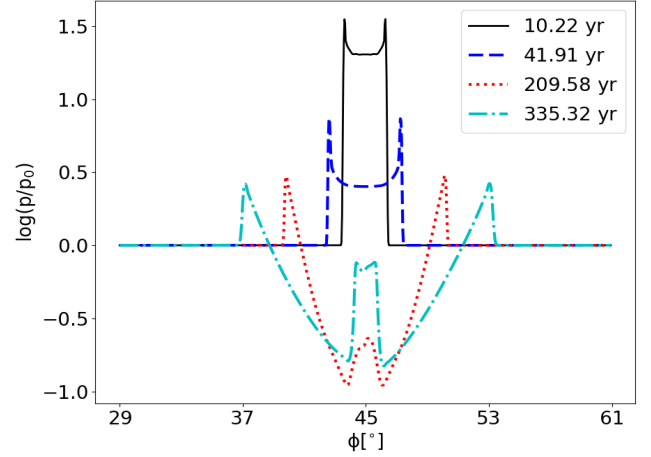


FIG. 12.— Azimuthal distribution of the gas pressure at  $z = 0$  and  $r = R_{\text{SNe}}$  in model 2 ( $\gamma = 1.1$ ).

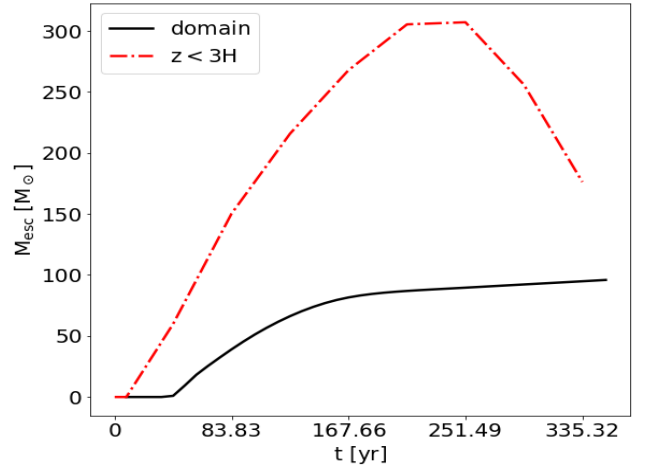


FIG. 13.— Same as Figure 9 but for model 2.

we carried out a simulation with all the same parameters except  $E_{51} = 78$  and  $\gamma = 1.4$ . We measured  $W_{\max} = 0.04$  pc in our simulation, which agrees with  $W_{\max}^{A,\text{trans}}$ . On the other hand,  $W_{\max}^{A,\text{shear}}$  still underestimates the width by a factor of 2.

In the following, we evaluate  $\mathcal{J}_{\text{SNe}}$ , that is the amount of angular momentum transported outward across a circle of radius  $R_{\text{SNe}}$ . More specifically, we give  $\beta_A$  (see §3.4), which is related to  $\mathcal{J}_{\text{SNe}}$  by

$$\beta_A = \frac{\mathcal{J}_{\text{SNe}}}{0.6(E_{\text{SNe}}\tilde{\Sigma})^{1/2}\tilde{H}R_{\text{SNe}}} \quad (30)$$

(see Equation 26). In order to determine  $\beta_A$ , we have measured  $\mathcal{J}_{\text{SNe}}(t)$  in our simulations. The remainder of the variables in Equation (30) are known input parameters. Since we are simulating the upper half of the disk, we include a factor of 2 in the calculation of  $\mathcal{J}_{\text{SNe}}$ . The resultant  $\beta_A$  in models 1 and 2 are shown in Figure 14. We see that  $\beta_A$  increases over time following a power law. In an inviscid disk, the value of  $\beta_A$  is expected to con-

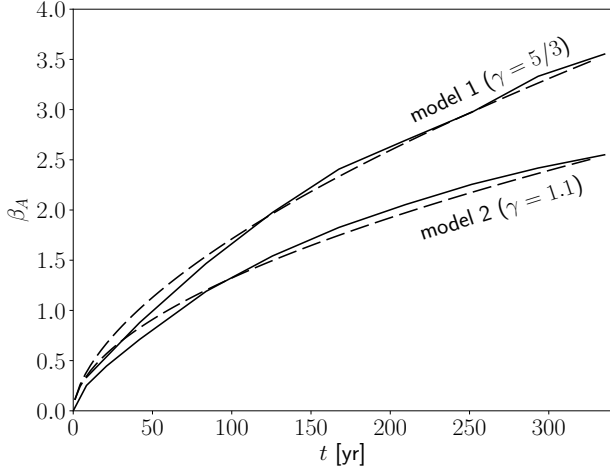


FIG. 14.—  $\beta_A$  vs. time (solid lines), overplotted with the fits  $\beta \propto t^l$  (dashed lines). The power-law indices are  $l = 0.6$  and  $l = 0.54$  for model 1 and model 2, respectively.  $\beta_A$  is given in Equation (30) and is a measurement of the transport of angular momentum by a single SN explosion. 2D simulations indicate that for the parameters used in these simulations, the angular momentum ceases to drift outward  $\sim 1P_{\text{orb}}$  after the explosion. Consistent with this result, we find that, in our 3D simulations, the rms azimuthal component of perturbed velocity  $\delta v_\phi$  in the shell decays with a characteristic timescale of  $0.7P_{\text{orb}}$ . Using the power-law fits shown in Figure 14, we evaluate the value of  $\beta_A$  at  $1P_{\text{orb}} = 838$  yr to obtain that  $\beta_A \simeq 6$  in model 1, and  $\beta_A \simeq 4$  in model 2. We will use these estimates of  $\beta_A$  in Section 5 when we study the effect of repeated SN explosions in the accretion disk.

To illustrate how the angular momentum transport occurs in the midplane of the disk, we calculate

$$\langle \alpha_{\text{inst}} \rangle \equiv \langle T_{R,\phi} \rangle / \langle p \rangle, \quad (31)$$

where  $T_{R,\phi} = \rho v_R \delta v_\phi$  is the Reynolds stress,  $p$  is the gas pressure and  $\langle \dots \rangle$  indicates averaging over  $\phi$ . Figure 15 shows the  $\langle \alpha_{\text{inst}} \rangle$  coefficient at the midplane for models 1 and 2 at two different times. Integrated over  $R$ ,  $\langle \alpha_{\text{inst}} \rangle$  is positive, signifying that the net transport of angular momentum is outwards. We also observe that  $\langle \alpha_{\text{inst}} \rangle$  at  $R = R_{\text{SNe}} = 0.2$  pc decreases over time.

##### 5. REPEATED SN EXPLOSIONS: THE VISCOSITY PARAMETER $\alpha$ IN STEADY STATE

In the previous Sections, we have calculated the amount of angular momentum that a single SN explosion can transport outwards. The effect of many SN explosions can be represented as an effective viscosity  $\alpha_{\text{SNe}}$ . As said in §2, other agents besides SN explosions, may be at work in AGN accretion disks that contribute to the effective viscosity of the disk  $\alpha$ . The redistribution of angular momentum by SN explosions will be the major contributor to the viscosity if  $\alpha_{\text{SNe}} \simeq \alpha$ . Given the rate of SN explosions per unit area in the disk  $\dot{n}_{\text{SNe}}$ , we can evaluate  $\alpha_{\text{SNe}}$ . This will be done in the next Sections.

###### 5.1. Contribution of SN explosions to $\alpha$

We can always express the redistribution of angular momentum through a radial flux  $F_J(R, t)$ . We will use

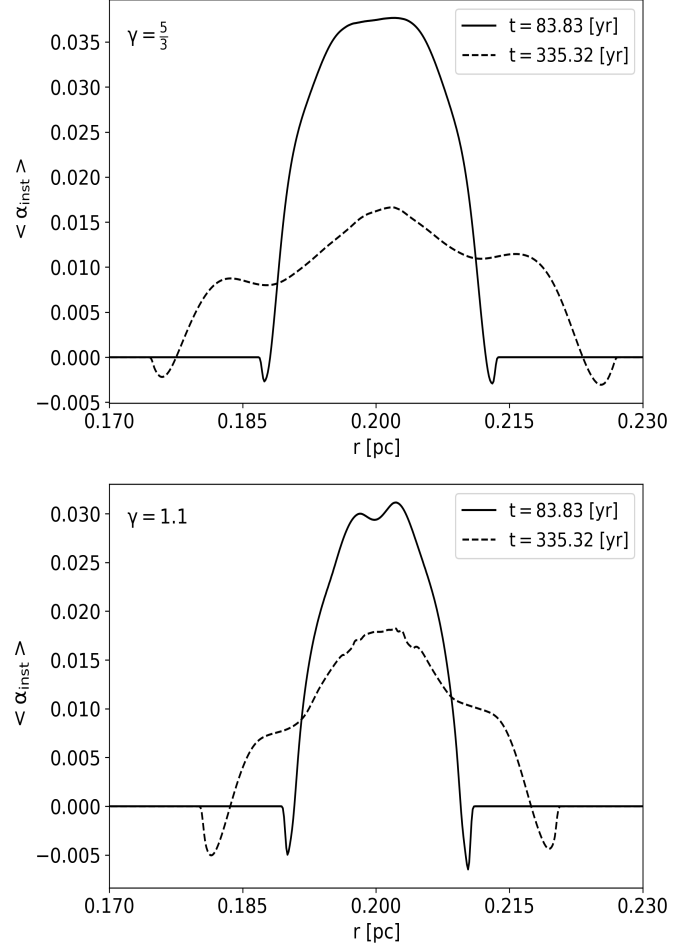


FIG. 15.— Radial profile of  $\langle \alpha_{\text{inst}} \rangle$  at  $t = 83.83$  yr and  $t = 335.3$  yr in model 1 (top) and in model 2 (bottom). The azimuthal average was done in our computational domain  $0 \leq \phi \leq \pi/2$ . Averaging between 0 and  $2\pi$  would result in a lower  $\langle \alpha_{\text{inst}} \rangle$  by a factor of 4.

the convention that  $F_J(R, t) > 0$  implies that the transport of angular momentum is outwards. If this flux were carried by density waves in a non-dissipative medium, then the angular momentum can be transported to infinity without deposition into the disk. However, in our case, the redistribution of angular momentum occurs at scales of the order of  $W$ . Following Goodman & Rafikov (2001), we may write the flux driven by SN explosions as

$$F_J(R) = 2\pi \int R_{\text{SNe}} \dot{n}_{\text{SNe}} \mathcal{J}_{\text{SNe}} \phi(R - R_{\text{SNe}}) dR_{\text{SNe}}, \quad (32)$$

where  $\phi(x)$  is a dimensionless distribution function with thickness  $\sim 2W_{\text{max}}$  and  $\phi(0) = 1$ ; it accounts for the damping length for the deposition of angular momentum. We may approximate the flux as

$$F_J(R) \simeq 4\pi \dot{n}_{\text{SNe}} W_{\text{max}} R \mathcal{J}_{\text{SNe}} \quad (33)$$

The expected rate of SN explosions can be estimated as  $\dot{n}_{\text{SNe}} = f_{\text{SNe}} \dot{\Sigma}_*$ , where  $\dot{\Sigma}_*$  is the star formation rate per unit area and  $f_{\text{SNe}}$  is the number of massive stars per solar mass of the star formation. To estimate  $f_{\text{SNe}}$ , we assume a Salpeter initial mass function with the low mass cut-off at  $0.1M_\odot$ . We have  $f_{\text{SNe}} = 0.01M_\odot^{-1}$ .

In order to estimate the viscosity parameter, we consider that the angular momentum flux in a steady-state Keplerian disk has the form

$$F_J(R) = 3\pi\alpha_{\text{SNe}}c_s H\Sigma R^2\Omega. \quad (34)$$

By equating Eqs. (33) and (34), we find

$$\alpha_{\text{SNe}} \simeq \frac{4}{3}f_{\text{SNe}} \left( \frac{W_{\text{max}}}{R} \right) \left( \frac{\dot{\Sigma}_\star}{\Sigma} \right) \left( \frac{\mathcal{J}_{\text{SNe}}}{c_s^2} \right). \quad (35)$$

In the next Section, we estimate  $\alpha_{\text{SNe}}$  in the SG model. To do so, we need the star formation rate  $\dot{\Sigma}_\star$ .

### 5.2. Application to the SG model

Assuming that stellar feedback is the main agent to provide vertical support to the disk, we can infer the required star formation rate per unit area, denoted by  $\dot{\Sigma}_\star^{\text{sup}}$  (see Appendix A). Figure 16 shows  $\dot{\Sigma}_\star^{\text{sup}}$  for our fiducial parameters. As discussed in TQM, the star formation rate has a bump where the opacity is low (in the ‘opacity gap’). In our case, the disk becomes optically thin at  $R_3 > 10$ .

As anticipated in §2 and discussed in detail in TQM, a large  $\dot{\Sigma}_\star^{\text{sup}}$  makes it difficult to fuel the central SMBH, as star formation may halt gas accretion onto the central SMBH (starvation). More specifically, star formation produces starvation if

$$\dot{M}_{\text{acc}} \leq 2\pi(1 + f_{\text{SNe}}M_{\text{exp}}) \int_{R_{\text{min}}}^{R_{\text{max}}} \dot{\Sigma}_\star R dR, \quad (36)$$

where  $R_{\text{min}} = 10^3 R_{\text{Sch}}$ ,  $R_{\text{max}} = 10^5 R_{\text{Sch}}$ ,  $M_{\text{exp}}$  is the mass expelled from the disk to the corona by one SN explosion.

Consider the phenomenological Kennicutt-Schmidt law  $\dot{\Sigma}_\star = C_{\text{KS}}\Sigma^{7/5}$ , where  $\Sigma$  is in unit of  $M_\odot\text{pc}^{-2}$  and  $\dot{\Sigma}_\star$  in  $M_\odot\text{pc}^{-2}\text{yr}^{-1}$  (Kennicutt 1998; Chen et al. 2009). Using Equations (2), (5) and (36), it is easy to show that in order to avoid starvation we need  $C_{\text{KS}} < C_{\text{cr}}$ , where

$$C_{\text{cr}} = 1.5 \times 10^{-10} \alpha_{0.1} g_{\text{SNe}}^{-1} Q_m^{0.93} \xi^{0.53} M_8^{-0.07}, \quad (37)$$

with  $g_{\text{SNe}} \equiv 1 + f_{\text{SNe}}M_{\text{exp}}$ .

In Figure 16 we can compare  $\dot{\Sigma}_\star^{\text{cr}} \equiv C_{\text{cr}}\Sigma^{7/5}$  and  $\dot{\Sigma}_\star^{\text{sup}}$ . We clearly see that  $\dot{\Sigma}_\star^{\text{cr}}$  is not enough to provide support to the disk and additional sources of feedback/heating are required.

Substituting Eq. (26) into Eq. (35), and generously assuming  $\dot{\Sigma}_\star = \dot{\Sigma}_\star^{\text{cr}}$ , we get the following upper value

$$\alpha_{\text{SNe}}^{(A)} \simeq 1 \times 10^{-3} \beta_A \xi^{0.53} \alpha_{0.1} g_{\text{SNe}}^{-1} M_8 E_{51}^{0.5} R_3^{1.15} \left( \frac{W_{\text{max}}}{R} \right) \quad (38)$$

in scenario A. In the above equation we have used  $f_{\text{SNe}} = 0.01 M_\odot^{-1}$ .

On the other hand, combining Eq. (27) and Eq. (35), we arrive at the following equation

$$\alpha_{\text{SNe}}^{(B)} \simeq 1.3 \times 10^{-3} \beta_B \alpha_{0.1} g_{\text{SNe}}^{-1} \hat{M}_{10}^{1/2} E_{51}^{1/2} R_3^{2/5} \left( \frac{W_{\text{max}}}{R} \right) \quad (39)$$

in scenario B. We recall that the equations above are valid as long as  $\alpha_{\text{SNe}} \leq \alpha$ .

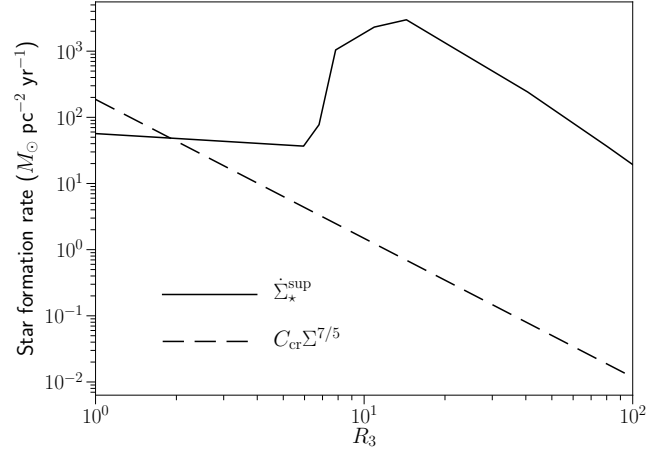


FIG. 16.— Radial profile of  $\dot{\Sigma}_\star^{\text{sup}}$  (solid line) and a Kennicutt-Schmidt law  $C_{\text{cr}}\Sigma^{7/5}$  (dashed line). We have used the following parameters:  $M_8 = 1$ ,  $\alpha_{0.1} = 1$ ,  $\xi = 0.3$ ,  $Q_m = 1$  and  $M_{\text{exp}} = 100M_\odot$ .

We see that the upper values for  $\alpha_{\text{SNe}}^{(A)}$  and  $\alpha_{\text{SNe}}^{(B)}$  do not explicitly depend on the precise value adopted for  $Q_m$ , but they depend weakly on  $Q_m$  through  $W_{\text{max}}$  (see, e.g., Eqs. 17, 19, C9 and C10).

Now, we evaluate  $\alpha_{\text{SNe}}^{(A)}$  for our reference values  $\alpha_{0.1} = 1$ ,  $Q_m = 1$ ,  $M_8 = 1$ ,  $\xi = 0.3$ ,  $E_{51} = 2$  and  $\gamma = 5/3$ . For these parameters, we have found in Section 4 that  $\beta_A \simeq 6$ ,  $M_{\text{exp}} = 300M_\odot$  and  $W_{\text{max}} \sim 0.1$  pc. For these values, Equation (38) implies  $\alpha_{\text{SNe}}^{(A)} \simeq 0.02$  and, therefore, SN explosions may contribute up to  $\sim 20\%$  to the effective viscosity in this model.

For  $\gamma = 1.1$ ,  $\alpha_{0.1} = 1$ ,  $M_8 = 1$ ,  $\xi = 0.3$ ,  $E_{51} = 2$ ,  $\beta_A \simeq 4$ ,  $M_{\text{exp}} = 100M_\odot$  and  $W_{\text{max}} \sim 0.075$  pc, we find a similar value of  $\alpha_{\text{SNe}}^{(A)} \simeq 0.02$ .

Interestingly,  $\alpha_{\text{SNe}}^{(A)}$  increases with  $M_8$ . More specifically, since  $W_{\text{max}}^{\text{shear}} \propto M_8^{8/9}$  (Equation 19) and  $R \propto M_8 R_3$ , Equation (38) predicts  $\alpha_{\text{SNe}}^{(A)} \propto M_8^{8/9}$ . Therefore,  $\alpha_{\text{SNe}}^{(A)} \simeq \alpha$  if  $M_8 \simeq 5$ .

In scenario B, we do not have an estimate of  $\beta_B$  but certainly  $\beta_B \leq 1$  (see Appendix C). If we generously take  $\beta_B = g_{\text{SNe}} = 1$ , Equation (39) with  $\alpha_{0.1} = 1$ ,  $M_8 = 1$ ,  $E_{51} = 2$ ,  $\hat{M}_{10} = 1$ ,  $W_{\text{max}}/R \sim 0.05$ ,  $R_3^{2/5} \simeq 6.5$  and  $\xi = 0.3$ , implies  $\alpha_{\text{SNe}}^{(B)} \simeq 6 \times 10^{-4}$ . This small value of  $\alpha_{\text{SNe}}^{(B)}$  compared to  $\alpha$  means that SN explosions are not efficient to drive the effective viscosity in this model and other sources need to be invoked.

In scenario B, the effective  $\alpha_{\text{SNe}}$  viscosity depends weakly on  $M_8$ . For illustration, consider a disk around a black hole with  $M_8 \ll 1$ . In this case we are in the limit  $\Delta \gg H$  (Appendix B). From Equation (B6) with  $\chi' \propto M_8$ , we have  $W_{\text{max}} \propto M_8^{8/9}$ . Since  $R \propto M_8 R_3$ , we get  $\alpha_{\text{SNe}}^{(A)} \propto (W_{\text{max}}/R) \propto M_8^{-1/9}$ .

Our result that  $\alpha_{\text{SNe}}^{(B)} \simeq 6 \times 10^{-4}$  for  $\xi = 0.3$ ,  $M_8 = 1$  and a SN rate of  $8 \times 10^{-3} \text{ yr}^{-1}$ , contrasts with the findings of Różyczka et al. (1995) that  $\alpha_{\text{SNe}} \simeq 0.1$  for  $M_8 = 1$  and a SN rate of  $10^{-4} \text{ yr}^{-1}$  in scenario B. Różyczka et al. (1995) overestimated  $\alpha_{\text{SNe}}$  because they implicitly assumed that the flow carries the angular momentum with-

out any dissipation. A finite damping length leads to a smaller effective viscosity, since angular momentum is deposited in the disk.

## 6. SUMMARY AND CONCLUSIONS

We have studied the role of SN explosions on the density structure and angular momentum redistribution in AGN accretion disks within a 1 pc scale. In our models, the AGN accretion disk properties are taken from the accretion disk model derived by SG. A SN explosion drives a shock that sweeps up mass, forms a cavity in the disk and redistributes disk angular momentum. We have provided some analytical estimates of the width of the cavity and the redistribution of angular momentum induced by a single SN explosion. We have introduced some fudge factors to include deviations from our simple approximations. By means of 3D hydrodynamical simulations, which take into account the lost mass and the momentum carried by the outflow, we have calibrated these fudge factors.

The radial width of the cavity, the mass ejected from the disk and the amount of angular momentum that is redistributed in the disk ( $\mathcal{J}_{\text{SNe}}$ ) by a single SN explosion all depend upon the value adopted for the adiabatic index  $\gamma$  of the gas. As a reference number, for  $\gamma = 1.1$ , we find  $\mathcal{J}_{\text{SNe}} \sim 8 \times 10^{60} \text{ g cm}^2 \text{ s}^{-1}$  for a SN explosion at a radius 0.2 pc, in our disk model with  $M_8 = 1$ .

We have estimated the effective  $\alpha_{\text{SNe}}$  viscosity provided by SN explosions in a steady state, where the rate of SN explosions is determined by adopting a Kennicutt-Schmidt law for the star formation. For  $\gamma$  between 1.1 and 5/3, we find that  $\alpha_{\text{SNe}} \gtrsim 0.1$  if  $M_8 \gtrsim 5$ .

Some authors adopted the momentum conservation limit to infer  $\alpha_{\text{SNe}}$  (e.g., Różyczka et al. 1995; Collin & Zahn 1999). In this limit, which is relevant when cooling is already important in the final stages of the free expansion phase, we find  $\alpha_{\text{SNe}}/\alpha \lesssim 6 \times 10^{-3}$ . Therefore, the contribution of SN explosions to the effective viscosity is negligible.

We have assumed that SN explosions occur in a smooth disk. However, unless the stellar heating is effective, the disk may fragment into clouds through gravitational instabilities (e.g., Jiang & Goodman 2011). If SN explosions occur inside dense clouds, part of their initial momentum will be absorbed by their natal clouds. Therefore, our estimates of  $\alpha_{\text{SNe}}$  should be treated as upper limits.

We thank the anonymous reviewer for helpful and constructive comments. AM-B and PFV acknowledge financial support from DGAPA-PAPIIT (UNAM) grant IG100218. FJS-S thanks PAPIIT for financial support through the project IN111118. ROC acknowledges post-doctoral CONACyT grant.

## APPENDIX

### A. PRESSURE DISTRIBUTION AND STAR FORMATION RATE

Following TQM, we can make predictions about the relative importance of thermal, radiation and turbulent pressure and their dependence with distance. We can also calculate the star formation rate per unit area. The equation of vertical equilibrium (Equation 39 in TQM) becomes

$$\rho_0 c_s^2 = p_{\text{th}} + \mathcal{E} \dot{\Sigma}_*^{\text{sup}} c \left( \frac{\tau}{2} + \lambda \right), \quad (\text{A1})$$

where  $\mathcal{E}$  is the efficiency with which star formation converts rest mass into radiation and  $\lambda$  is a dimensionless parameter that measures the amount of the momentum injected by stars that is converted into turbulent motions ( $c$  is the light speed). To compute  $p_{\text{th}}$ , we evaluate the gas temperature  $T$  through

$$T^4 = \frac{3}{4} T_{\text{eff}}^4 \left( \tau + \frac{2}{3\tau} + \frac{4}{3} \right), \quad (\text{A2})$$

where  $\tau = \kappa \Sigma / 2$ ,  $\kappa$  is the disk opacity and

$$\sigma_{\text{SB}} T_{\text{eff}}^4 = \frac{1}{2} \mathcal{E} \dot{\Sigma}_*^{\text{sup}} c^2 + \frac{3}{8\pi} \dot{M}_{\text{acc}} \Omega^2. \quad (\text{A3})$$

Here  $\sigma_{\text{SB}}$  is the Stefan-Boltzmann constant. Assuming  $\mathcal{E} = 10^{-3}$ ,  $\lambda = 1$ , and the disk opacities given in TQM, which are based on Semenov et al. (2003), we can derive  $\dot{\Sigma}_*^{\text{sup}}$ ,  $p_{\text{th}}$ ,  $p_{\text{rad}}$  and  $p_{\text{tur}}$  in our disk model. We note that  $p_{\text{rad}} = \mathcal{E} \tau \dot{\Sigma}_*^{\text{sup}} c / 2$  and  $p_{\text{tur}} = \lambda \mathcal{E} \dot{\Sigma}_*^{\text{sup}} c$ . To easy comparison, we have taken the same values for  $\mathcal{E}$  and  $\lambda$  as TQM, but we warn that they are uncertain.

### B. MAXIMUM RADIAL WIDTH OF THE SNR IN THE LIMIT $\Delta \gg \tilde{H}$

As pointed out in Section 3.1, in some cases (especially for  $M_8 < 1$ ), the SN explosion can break out of the disk in the free expansion phase. In cases in which  $\Delta \gg \tilde{H}$ , this free expansion phase continues until  $R_{\text{sh}} \simeq \Delta$ . We assume that a momentum conservation phase begins just after the free expansion phase ends. Only the momentum of those elements ejected in a polar angle  $\hat{\theta}$  between  $\hat{\theta}_{\text{min}} \simeq \arccos(\tilde{H}/(\sqrt{\Delta^2 + \tilde{H}^2}))$  and  $\hat{\theta}_{\text{max}} \simeq \pi - \arccos(\tilde{H}/(\sqrt{\Delta^2 + \tilde{H}^2}))$  will be able to push the disk along the planar directions. Thus, the momentum absorbed by the disk will be

$$P_{\text{abs}} \simeq \frac{P_{\text{SNe}}}{4\pi} \int_0^{2\pi} \int_{\hat{\theta}_{\text{min}}}^{\hat{\theta}_{\text{max}}} \sin^2 \hat{\theta} d\theta d\phi = P_{\text{SNe}} \frac{\tilde{H}}{\sqrt{\Delta^2 + \tilde{H}^2}}. \quad (\text{B1})$$

It is easy to show that the mass that escapes from the disk is  $\simeq 0.5\pi\tilde{\Sigma}\Delta^2$ . Momentum conservation implies that  $\dot{R}_{\text{sh}}$  obeys

$$\pi\tilde{\Sigma}\left(R_{\text{sh}}^2 - \frac{\Delta^2}{2}\right)\dot{R}_{\text{sh}} = \chi' P_{\text{SNe}}, \quad (\text{B2})$$

with  $\chi' \equiv \tilde{H}/\sqrt{\Delta^2 + \tilde{H}^2}$ . The transonic condition (see §3.3) occurs when the width of the SNR in the radial direction is

$$W_{\text{max}}^{\text{trans}} \simeq 2\left(\frac{\chi' P_{\text{SNe}}}{\pi\tilde{\Sigma}\tilde{c}_s} + \frac{\Delta^2}{2}\right)^{1/2}. \quad (\text{B3})$$

On the other hand,  $W_{\text{max}}^{\text{shear}}$  satisfies a cubic equation. Here we just provide a lower limit:

$$W_{\text{max}}^{\text{shear}} > 1.5\left(\frac{\chi' P_{\text{SNe}}}{\tilde{\Sigma}\tilde{\Omega}}\right)^{1/3}. \quad (\text{B4})$$

We notice that  $W_{\text{max}}^{\text{trans}}$  and  $W_{\text{max}}^{\text{shear}}$  do not depend explicitly on  $E_{\text{SNe}}$  because the adiabatic phase never develops.

In our disk model (Eqs. 5-7), approximating  $\chi' \simeq \tilde{H}/\Delta$ , the widths read

$$W_{\text{max}}^{\text{trans}} = 10^{-3}\xi^{-1/12}Q_{\text{m}}^{1/3}M_8^{2/3}\hat{M}_{10}^{1/2}E_{51}^{1/4}\tilde{R}_3^{9/8}(1 + 4 \times 10^{-3}\xi^{-1/6}Q_{\text{m}}^{1/3}M_8^{-2/3}\tilde{R}_3^{-3/4})^{1/2}\text{pc}, \quad (\text{B5})$$

and

$$W_{\text{max}}^{\text{shear}} > 4.5 \times 10^{-4}\chi'^{1/3}\xi^{-1/9}Q_{\text{m}}^{2/9}M_8^{5/9}\hat{M}_{10}^{1/6}E_{51}^{1/6}\tilde{R}_3\text{pc}. \quad (\text{B6})$$

### C. MAXIMUM RADIAL WIDTH OF THE SNR IN SCENARIO B

Scenario B assumes that the internal pressure in the cavity is negligible and, therefore, the SNR evolves as a pure momentum-driven snowplow. We will distinguish between cases where the SN explosion occurs within the radius  $\tilde{R}_b^{(B)}$  and beyond  $\tilde{R}_b^{(B)}$ .

**Case  $\tilde{R}_3 > \tilde{R}_b^{(B)}$ .** Since the SNR cannot breakout of the disk, it will hardly reach a height larger than  $\simeq \sqrt{3}\tilde{H}$ . Momentum-conservation dictates

$$P_{\text{SNe}} \simeq \frac{4\pi}{3}\tilde{\rho}_0 R_{\text{sh}}^3 \dot{R}_{\text{sh}}. \quad (\text{C1})$$

The transonic and shear conditions imply

$$W_{\text{max}}^{B,\text{trans}} \simeq 1.2\left(\frac{P_{\text{SNe}}}{\tilde{\rho}_0\tilde{c}_s}\right)^{1/3}, \quad (\text{C2})$$

and

$$W_{\text{max}}^{B,\text{shear}} \simeq 1.5\left(\frac{P_{\text{SNe}}}{\tilde{\rho}_0\tilde{\Omega}}\right)^{1/4}. \quad (\text{C3})$$

In terms of  $M_8$  and  $\tilde{R}_3$ ,

$$W_{\text{max}}^{B,\text{trans}} = 5 \times 10^{-4}\xi^{-1/9}Q_{\text{m}}^{2/9}M_8^{5/9}\hat{M}_{10}^{1/6}E_{51}^{1/6}\tilde{R}_3\text{pc}, \quad (\text{C4})$$

and

$$W_{\text{max}}^{B,\text{shear}} = 2 \times 10^{-4}Q_{\text{m}}^{1/4}M_8^{3/4}\hat{M}_{10}^{1/8}E_{51}^{1/8}\tilde{R}_3^{9/8}\text{pc}. \quad (\text{C5})$$

**Case  $\tilde{R}_3 < \tilde{R}_b^{(B)}$ .** If the explosion site lies at a radius less than  $\tilde{R}_b^{(B)}$ , the SNR is able to break out of the disk. After breakout, i.e. when  $R_{\text{sh}} \gtrsim \sqrt{3}\tilde{H}$ , the shock velocity is given by

$$\chi_B P_{\text{SNe}} = \pi R_{\text{sh}}^2 \tilde{\Sigma} \dot{R}_{\text{sh}}. \quad (\text{C6})$$

Here  $\chi_B$  is the fraction of momentum that is absorbed by the disk; thus  $\chi_B \leq 1$ . Imposing the transonic and shear conditions, it follows that

$$W_{\text{max}}^{B,\text{trans}} \simeq \left(\frac{\chi_B P_{\text{SNe}}}{\tilde{\Sigma}\tilde{c}_s}\right)^{1/2}, \quad (\text{C7})$$

and

$$W_{\text{max}}^{B,\text{shear}} \simeq 1.5\left(\frac{\chi_B P_{\text{SNe}}}{\tilde{\Sigma}\tilde{\Omega}}\right)^{1/3}. \quad (\text{C8})$$

For our accretion disk model (Eqs. 5-7),

$$W_{\text{max}}^{B,\text{trans}} \simeq 10^{-3}\chi_B^{1/2}\xi^{-1/3}Q_{\text{m}}^{1/6}M_8^{1/6}\hat{M}_{10}^{1/4}E_{51}^{1/4}\tilde{R}_3^{3/4}\text{pc}, \quad (\text{C9})$$

and

$$W_{\max}^{B,\text{shear}} \simeq 4.5 \times 10^{-4} \chi_B^{1/3} \xi^{-1/9} Q_m^{2/9} M_8^{5/9} \hat{M}_{10}^{1/6} E_{51}^{1/6} \tilde{R}_3 \text{ pc.} \quad (\text{C10})$$

## REFERENCES

- Baldwin, J. A., Hamann, F., Korista, K. T., Ferland, G. J., Dietrich, M., & Warner, C. 2003, *ApJ*, 583, 649
- Begelman, M. C., & Silk, J. 2017, *MNRAS*, 464, 2311
- Bellovary, J. M., Mac Low, M.-M., McKernan, B., & Ford, K. E. 2016, *ApJ*, 819, L17
- Benítez-Llambay, P., & Masset, F. S. 2016, *ApJS*, 223, 11
- Bentz, M. C., Walsh, J. L., & Barth, A. J., et al. 2009, *ApJ*, 705, 199
- Chen, Y.-M., Wang, J.-M., Yan, C.-S., Hu, C., & Zhang, S. 2009, *ApJ*, 695, L130
- Collin, S., & Huré, J.-M. 2001, *A&A*, 372, 50
- Collin, S., & Zahn, J.-P. 1999, *A&A*, 344, 433
- Collin, S., & Zahn, J.-P. 2008, *A&A*, 477, 419
- Czerny, B., Du, P., Wang, J.-M., & Karas, V. 2016, *ApJ*, 832, 15
- de Val-Borro, M., Edgar, R. G., Artymowicz, P. et al. 2006, *MNRAS*, 370, 529
- Dietrich, M., Hamann, F., Shields, J. C., et al. 2003, *ApJ*, 589, 722
- Dittmann, A. J., & Miller, M. C. 2020, *MNRAS*, 493, 3732
- Du, P., & Wang, J.-M. 2019, *ApJ*, 886, 42
- Ferrara, A., & Tolstoy, E. 2000, *MNRAS*, 313, 291
- Gammie, C. F. 2001, *ApJ*, 553, 174
- Goodman, J. 2003, *MNRAS*, 339, 937
- Goodman, J., & Rafikov, R. R. 2001, *ApJ*, 552, 793
- Hamann, F., & Ferland, G. 1993, *ApJ*, 418, 11
- Hobbs, A., Nayakshin, S., Power, C., & King, A. 2011, *MNRAS*, 413, 2633
- Hopkins, P. F., & Quataert, E. 2011, *MNRAS*, 415, 1027
- Hopkins, P. F., Hayward, C. C., Narayanan, D., & Hernquist, L. 2012, *MNRAS*, 420, 320
- Jiang, Y.-F., & Goodman, J. 2011, *ApJ*, 730, 45
- Jiang, L., Fan, X., Vestergaard, M., Kurk, J. D., Walter, F., Kelly, B. C., & Strauss, M. A. 2007, *AJ*, 134, 1150
- Juarez, Y., Maiolino, R., Mujica, R., et al. 2009, *A&A*, 494, L25
- Kaspi, S., Brandt, W. N., Maoz, D., Netzer, H., Schneider, D. P., & Shemmer, O. 2007, *ApJ*, 659, 997
- Kawakatu, N., & Wada, K. 2008, *ApJ*, 681, 73
- Kennicutt, R. C. Jr. 1998, *ApJ*, 498, 541
- Kompaneets, A. S. 1960, *Dokl. Akad. Nauk. SSSR*, 130, 1001 [Soviet Phys. Dokl, 5, 46 (1960)]
- Kurk, J. D., Walter, F., Fan, X., et al. 2007, *ApJ*, 669, 32
- Larson, R. B. 1990, *MNRAS*, 243, 588
- Mac Low, M.-M., & Ferrara, A. 1999, *ApJ*, 513, 142
- Mac Low, M.-M., McGray, R., & Norman, M. L. 1989, *ApJ*, 337, 141
- McKernan, B., Ford, K. E. S., Lyra, W., & Perets, H. B. 2012, *MNRAS*, 425, 460
- Meru, F., Juhász, A., Ilee, D. et al. 2017, *ApJ*, 839, L24
- Mishra, B., Begelman, M. C., Armitage, P. J., & Simon, J. B. 2020, *MNRAS*, 492, 1855
- Nagao, T., Marconi, A., & Maiolino, R. 2006, *A&A*, 447, 157
- Olano, C. A. 1982, *A&A*, 112, 195
- Olano, C. A. 2009, *A&A*, 506, 1215
- Palous, J., Franco, J., & Tenorio-Tagle, G. 1990, *A&A*, 227, 175
- Paczynski, B. 1978, *Acta Astron.*, 28, 91
- Pariev, V. I., Blackman, E. G., & Boldyrev, S. A. 2003, *A&A*, 407, 403
- Rafikov, R. R. 2009, *ApJ*, 704, 281
- Różyczka, M., Bodenheimer, P., & Lin, D. N. C. 1995, *MNRAS*, 276, 597
- Sawada, K., Matsuda, T., & Hachisu, I. 1986, *MNRAS*, 219, 75
- Secunda, A., Bellovary, J., Mac Low, M.-M., Ford, K. E. S., McKernan, B., Leigh, N. W. C., Lyra, W., & Sándor, Z. 2019, *ApJ*, 878, 85
- Semenov, D., Henning, T., Helling, C., Ilgner, M., & Sedlmayr, E. 2003, *A&A*, 410, 611
- Shakura, N. Z., & Sunyaev R. A., 1973, *A&A*, 24, 337
- Shlosman, I., & Begelman, M. C. 1987, *Nature*, 328, 810
- Shlosman, I., Begelman, M. C., & Frank, J. 1990, *Nature*, 345, 679
- Shlosman, I., Frank, J., & Begelman, M. C. 1989, *Nature*, 338, 45
- Silich, S. A. 1992, *Ap&SS*, 195, 317
- Sirko, E., & Goodman, J. 2003, *MNRAS*, 341, 501
- Tenorio-Tagle, G., & Palous, J. 1987, *A&A*, 186, 287
- Thompson, T. A., Quataert, E., & Murray, N. 2005, *ApJ*, 630, 197
- Wada, K., & Norman, C. A. 2002, *ApJ*, 566, L21
- Wang, J.-M., Du, P., Baldwin, J. A., Ge, J.-Q., Hu, C., & Ferland, G. J. 2012, *ApJ*, 746, 137
- Wang, J.-M., Ge, J.-Q., Hu, C., Baldwin, J. A., Li, Y.-R., & Ferland, G. J. 2011, *ApJ*, 793, 3
- Wang, J.-M., Yan, C.-S., Gao, H.-Q., Hu, C., Li, Y.-R., & Zhang, S. 2010, *ApJ*, 719, L148
- Warner, C., Hamann, F., & Dietrich, M. 2003, *ApJ*, 596, 72
- Yang, Y., Bartos, I., Haiman, Z., Kocsis, B., Márka, Z., Stone, N. C., & Márka, S. 2020, *ApJ*, 876, 122